Journal of Medicinal Chemistry

Article

pubs.acs.org/jmc

Conopeptide-Derived κ-Opioid Agonists (Conorphins): Potent, Selective, and Metabolic Stable Dynorphin A Mimetics with Antinociceptive Properties

Andreas Brust,[*,†,‡] Daniel E. Croker,[†,‡] Barbara Colless,[†,‡] Lotten Ragnarsson,[†,‡] Åsa Andersson,[†,‡] Kapil Jain,[‡] Sonia Garcia-Caraballo,[§] Joel Castro,[§] Stuart M Brierley,[§] Paul F. Alewood,[‡] and Richard J. Lewis[*,†,‡]

[†]Xenome Limited, Brisbane, Queensland 4068, Australia

[‡]Institute for Molecular Biosciences, The University of Queensland, Brisbane, Queensland, 4072, Australia

[§]Visceral Pain Group, Centre for Nutrition and Gastrointestinal Disease, Discipline of Medicine, The University of Adelaide, South Australian Health and Medical Research Institute, SAHMRI, Adelaide, SA 5000, Australia

Supporting Information

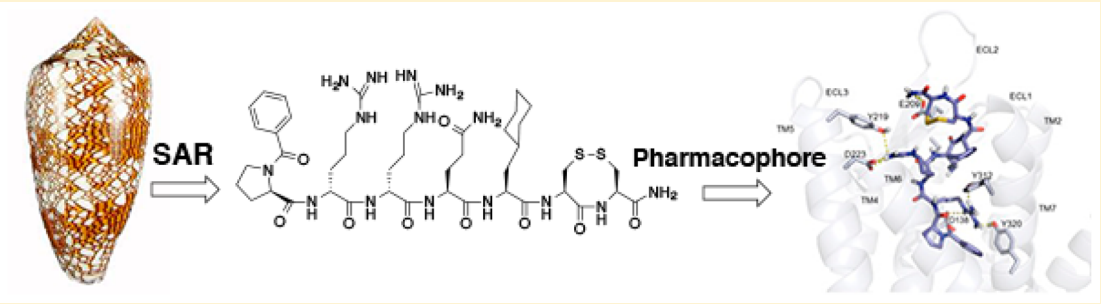

ABSTRACT: Opioid receptor screening of a conopeptide library led to a novel selective κ-opioid agonist peptide (conorphin T). Intensive medicinal chemistry, guided by potency, selectivity, and stability assays generated a pharmacophore model supporting rational design of highly potent and selective κ-opioid receptor (KOR) agonists (conorphins) with exceptional plasma stability. Conorphins are defined by a hydrophobic benzoprolyl moiety, a double arginine sequence, a spacer amino acid followed by a hydrophobic residue and a C-terminal vicinal disulfide moiety. The pharmacophore model was supported by computational docking studies, revealing receptor−ligand interactions similar to KOR agonist dynorphin A (1−8). A conorphin agonist inhibited colonic nociceptors in a mouse tissue model of chronic visceral hypersensitivity, suggesting the potential of KOR agonists for the treatment of chronic abdominal pain. This new conorphine KOR agonist class and pharmacophore model provide opportunities for future rational drug development and probes for exploring the role of the κ-opioid receptor.

INTRODUCTION

Marine natural products remain an important source of new chemical diversity for drug discovery.[1,2] Venoms from the genus *Conus* (marine cone snails) provide an enriched source of highly evolved bioactive compounds.[3] These predatory molluscs are equipped with a venom apparatus that produces a species-specific cocktail of peptides to immobilize prey that comprise fish, molluscs, or worms. It is estimated that the venom of a single *Conus* species typically contain in excess of 1000 unique venom peptides called conotoxins or conopeptides which translates to >500 000 potentially bioactive peptides across the genus.[3−5] Conotoxins are highly specific for membrane protein targets and usually possess constrained structures with multiple disulfide bonds.[3] The disulfide bond framework is interspersed by loops of amino acids that typically contain the binding residues presented in a well-defined three-dimensional space. The potency, selectivity, and chemical stability of conotoxins make these compounds attractive starting points for drug development.[6−11] In fact, several conotoxins are currently in clinical trials, with ω-conotoxin MVIIA (ziconotide)[12,13] on the market for the treatment of chronic pain.[12,13] On the basis of their untapped pharmacolgical potential,[14−18] we developed a synthetic conopeptide library[19] comprising >2000 peptides, from nucleotide derived venom peptide sequences to be used as a platform for novel drug lead discovery.

Opioid receptors are a major target for pain management.[20−24] Three opioid receptors have been cloned: the μ- (MOR), κ- (KOR), and δ- (DOR) opioid receptor.[25,26] In addition, the nociceptin/orphanin FQ receptor (NOP) is an "opioid-related" receptor that exhibits a high degree of structural homology to conventional opioid receptors despite having distinct pharmacology.[27,28] KOR is different from the

Received: June 14, 2015
Published: February 9, 2016

DOI: 10.1021/acs.jmedchem.5b00911
J. Med. Chem. 2016, 59, 2381−2395

other opioid receptors in terms of tissue expression patterns, functional properties, and side effect profile upon activation.[29] Morphine and related opiates are to date the most potent analgesics and predominantly modulate MOR expressed in the central nervous system. However, the effects at MOR expressed in the periphery contribute also to serious dose-limiting side effects.[30,31] In contrast to this, modulation of KOR in the CNS results in side effects such as hallucinations and disphoria.[29,32]

Development of peripherally restricted selective ligands for the KOR is of considerable therapeutic interest as potential analgesic.[29,32,33] In general KOR agonists are of interest for a variety of other therapeutic applications. KOR agonists produce analgesia without MOR agonist related side effects; in addition to their anti-inflammatory[34] and neuroprotective effects, they suppress the rewarding effects of opiates and cocaine.[35,36] KOR agonists also are potential therapeutics for pruritus,[37] depression,[38,39] opiate dependence,[36] and cocaine seeking behavior.[35,40] In particular KOR agonists have been shown to exert analgesic activity in a variety of visceral pain models mediated by peripherally expressed KOR, suggesting that a peripherally restricted KOR agonist might be useful treatment for a variety of visceral pain conditions, including postoperative pain, ileus, pancreatitis pain, dysmenorrhea, labor pain, and functional bowel disorders.[32,34,40,41] One such KOR agonist, asimadoline (*N*-[(1*S*)-2-[(3*S*)-3-hydroxypyrrolidin-1-yl]-1-phenylethyl]-*N*-methyl-2,2-diphenylacetamide),[42] appears to inhibit nociception via activation of KORs expressed on the peripheral endings of colonic nociceptors,[43] suggesting a peripherally restricted KOR agonist might be useful treatment for a variety of visceral pain conditions including irritable bowel syndrome (IBS).

Dynorphin A (YGGFLRRIRPKLKWDNQ or dynA (1−17)) is the endogenous agonist of human KOR. DynA (1−17) contains the N-terminal YGGF message sequence common to endogenous opioids, like endorphins and enkephalins, which contributes to opiate receptor affinity but not opiate receptor selectivity.[44] Removal of as many as nine residues from the C-terminus of dynA (1−17) has little effect on KOR activity.[45,46] In addition replacement of the nine C-terminal residues of dynA (1−17) with those of nociceptin also maintained activity at KOR.[47] From this it can be concluded that the essential pharmacophore of dynA (1−17) lies within the N-terminal fragment dynA (1−8) (YGGFLRRI). Docking simulations of dynA (1−8) binding to the KOR revealed a partially stabilized α-helix from Phe4 to Ile8, allowing the YGGF message domain to bind in a hydrophobic binding pocket comprising elements from transmembrane helices 3, 5, 6, and 7 of KOR.[48] The recent X-ray structure of KOR in complex with an antagonist (JDTic; (3*R*)-7-hydroxy-*N*-[(2*S*)-1-[(3*R*,4*R*)-4-(3-hydroxyphenyl)-3,4-dimethylpiperidin-1-yl]-3-methylbutan-2-yl]-1,2,3,4-tetrahydroisoquinoline-3-carboxamide)[49] has been used to confirm earlier docking results and is supported by receptor mutagenesis and functional studies.[50] The consensus view is that the YGGF message domain interacts with KOR in a similar way as the antagonist JDTic, encompassing a conserved opioid receptor hydrophobic pocket comprising W124$^{(ECL1)}$, V134$^{(3.28)}$, I135$^{(3.19)}$, and C210$^{(ECL2)}$. Additionally the D138$^{(3.32)}$ carboxylate interaction with the Y1-amine residue is also critical for high affinity interactions.[49] The dynA (1−8) KOR address domain LRRI presented in an extended conformation with multiple KOR interactions, with a Q115$^{(2.60)}$ to NH interaction at Leu5 of particular importance.[50] A prominent salt bridge between E297$^{(6.58)}$ and Arg7 residues in the address sequence of dynA (1−8) was also identified that likely contributes strongly to KOR receptor selectivity.[49,50]

Previous small molecule KOR agonist molecules (e.g., fedotozine, (2*R*)-*N*,*N*-dimethyl-2-phenyl-1-[(3,4,5-trimethoxybenzyl)oxy]-2-butanamine)[51] have failed in clinical development[51] due to limited selectivity/potency or significant blood−brain barrier penetration which led to unwanted central side effects.[51] However, the peripherally restricted KOR agonist asimadoline[42,52] is currently in phase 3 clinical trials for the treatment of pain associated with irritable bowel syndrome.[42,43] Peripherally restricted KOR agonists have been developed based on peptidic molecules[53,54] by CARA Therapeutics [D-Phe-D-Phe-D-Nle-D-Arg-NH-4-picolyl (CR665) and D-Phe-D-Phe-D-Leu-D-Lys-[γ-(4-*N*-piperidinyl)aminocarboxylic acid (CR845)][53,54] which combine high affinity, excellent selectivity, and limited or no central side effects and are currently undergoing phase 2 testing for postoperative pain.[53,54]

In the present study, a KOR agonist (**1**) named conorphin-T (sequence: NCCRRQICC) was identified from the screening of a *Conus* venom peptide library across the opiate receptors. Detailed structure−activity studies and medicinal chemistry optimization generated a new class of metabolically stable lead molecules that had subnanomolar affinity and high selectivity for KOR over the other opioid receptors. Here we describe the development and visceral analgesic efficacy of potent KOR agonist conorphins and the associated pharmacophore model that describes their binding to KOR.

RESULTS AND DISCUSSION

Library Screening and Initial Hit Identification. A synthetic peptide library containing over 2000 conopeptides from cDNA libraries obtained from venom duct preparations of cone shells was screened in a binding assay across a panel of human KOR, MOR, and DOR receptors. This screen revealed a previously uncharacterized nine amino acid peptide **1** we name conorphin-T, whose sequence was previously found in a cDNA library from *C. textile*.[55] **1** contains two disulfide bonds and was identified as a KOR agonist, without detectable binding at the other opioid receptors (Table 3).

By use of selective disulfide bond formation, the affinity of each individual disulfide isomer was assessed at KOR by radioligand binding assay. Peptide **1** in the bead form (1−2, 3−4 disulfide connectivity) (Figure 1, Table 1) was identified as the most active isomer at KOR, and its structure−activity was investigated to uncover more potent analogues suitable for further development. Selected synthetic analogues were

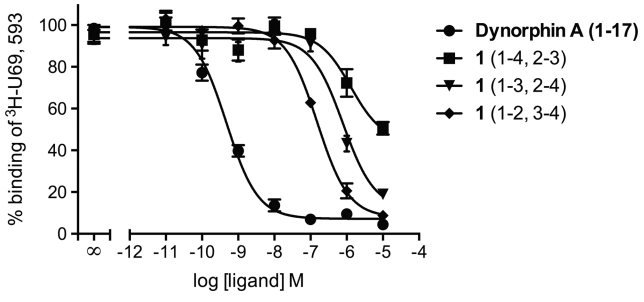

Figure 1. KOR affinity of **1** and its disulfide isomers. Data shown are the mean ± SEM values of at least three independent experiments each performed in triplicate.

DOI: 10.1021/acs.jmedchem.5b00911
J. Med. Chem. 2016, 59, 2381−2395

Table 1. Activity and Stability of Dynorphin, the Venom Library Conorphine (1), and Its Analogues 2−75[a]

compd	sequence	K_i ± SD (nM)	ERK EC_{50} ± SD (nM)	cAMP EC_{50} ± SD (nM)	$T_{1/2}$ plasma
dynorphin A (1−17)	YGGFLRRIRPKLKWDNQ-NH_2	0.28 ± 0.25	0.95 ± 0.34	1.2 ± 0.24	120 min
dynorphin A (1−13)	YGGFLRRIRPKLK-NH_2	0.40 ± 0.72			
1 (1−3, 2−4)	NCCRRQICC-NH_2	1474 ± 1965			
1 (1−4, 2−3)	NCCRRQICC-NH_2	580 ± 277			
1 (1−2, 3−4)	NCCRRQICC-NH_2	80.4 ± 42.6	9848 ± 3272	9446 ± 403	15 min
2	NCCARQICC-NH_2	170 ± 68			
3	NCCRAQICC-NH_2	406 ± 242			
4	NCCRRAICC-NH_2	133 ± 74			
5	NCCRRQACC-NH_2	2452 ± 515			
6	UCCRRQICC-NH_2	67.5 ± 6.7	5864 ± 3259	11.5 ± 1.7	15 min
7	YCCRRQICC-NH_2	40.3 ± 8.2			
8	RRQI-NH_2	23003 ± 9232			
9	NCCRRQI-NH_2	14662 ± 1542			
10	RRQICC-NH_2	270 ± 61			45 min
11	URRQICC-NH_2	191 ± 35	7486 ± 1701	1.9 ± 1.7	180 min
12	NCCRRQVCC-NH_2	664 ± 424			
13	NCCRRQLCC-NH_2	24.8 ± 3.9			
14	NCCRRQ[CHA]CC-NH_2	1.3 ± 1.1			<15 min
15	NCCRRQFCC-NH_2	28.4 ± 8.1			
16	NCCRRQ[NAL]CC-NH_2	2.9 ± 0.8			<15 min
17	NCCHRQICC-NH_2	137 ± 79			
18	NCCRHQICC-NH_2	85 ± 75.5			
19	NCCKRQICC-NH_2	426.9 ± 381			
20	NCCRKQICC-NH_2	208 ± 193			
21	NCC[CIT]RQICC-NH_2	218 ± 18			
22	NCCR[CIT]QICC-NH_2	387 ± 127			
23	URRQ[CHA]CC-NH_2	6.7 ± 1.1	1580 ± 439	15.2 ± 7.4	90 min
24	UrRQ[CHA]CC-NH_2	13 ± 5.3			90 min
25	URrQ[CHA]CC-NH_2	16.1 ± 9.3			1200 min
26	UrrQ[CHA]CC-NH_2	3.9 ± 1.5	1105 ± 839	12.6 ± 3.6	360 min
27	4F-Bz-rrQ[CHA]CC-NH_2	5.4 ± 1.7			
28	3Br-Bz-rrQ[CHA]CC-NH_2	5.3 ± 0.8			
29	3Cl-Bz-rrQ[CHA]CC-NH_2	6.7 ± 1.4			
30	4F-Bnz-rrQ[CHA]CC-NH_2	1.2 ± 0.3			
31	3Br-Bnz-rrQ[CHA]CC-NH_2	1.2 ± 0.7			
32	3Cl-Bnz-rrQ[CHA]CC-NH_2	2.1 ± 0.8			
33	[Anc]rrQ[CHA]CC-NH_2	0.64 ± 0.24			60 min
34	3-Qin-rrQ[CHA]CC-NH_2	0.71 ± 0.42			45 min
35	[TIC]rrQ[CHA]CC-NH_2	0.91 ± 0.35			45 min
36	[TIQ]rrQ[CHA]CC-NH_2	1.18 ± 0.36			45 min
37	Nz-PrrQ[CHA]CC-NH_2	0.07 ± 0.02			30 min
38	4Cl-Bz-PrrQ[CHA]CC-NH_2	0.13 ± 0.03			60 min
39	Bz-PrrQ[CHA]CC-NH_2	0.25 ± 0.13	0.36 ± 0.11	0.41 ± 0.11	240 min
40	4MeO-Bz-PrrQC[CHA]CC-NH_2	0.59 ± 0.14			120 min
41	3,4Cl-Bz-PrrQC[CHA]CC-NH_2	0.98 ± 0.2			60 min
42	4HO-Bz-PrrQC[CHA]CC-NH_2	1.2 ± 0.3			120 min
43	4-NO_2−Bz-PrrQC[CHA]CC-NH_2	2.2 ± 0.5			
44	UrrQ[CHA][PEN]C-NH_2	1.3 ± 0.5	450 ± 198	10.5 ± 3.2	100% at 24 h
45	Bz-PrrQ[CHA][PEN]C-NH_2	1140 ± 891			95% at 24 h
46	Bz-PrrQ[CHA][NMC]C-NH_2	15.2 ± 8.8			
47	Bz-PrrQ[CHA]-*CH2-NH*-CC-NH_2	135 ± 32			960 min
48	Bz-PrrQ[CHG]CC-NH_2	0.48 ± 0.22	0.62 ± 0.31	0.39 ± 0.23	1200 min
49	UrrQ[CHA][HCY]C-NH_2	783 ± 133			
50	UrrQ[CHA]C[HCY] -NH_2	1573 ± 822			
51	UrrQ[CHA][HCY][HCY] -NH_2	241 ± 31			
52	[TIC]rrQ[CHA][SEC][SEC] -NH_2	2.4 ± 0.3			360 min
53	UrrQ[CHA][SEC]C-NH_2	7.8 ± 1.7			360 min
54	Bz-PrrQ[CHA](D[DAP]) -NH_2	233 ± 90			
55	Bz-PrrQ[CHA]CC CH_2-NH_2 bridge	15.8 ± 9.7			
56	Bz-PrrQ[CHA]C[MEG] -NH_2	465 ± 311			
57	Bz-PrrQ[CHA][MEG]C-NH_2	199 ± 76			

DOI: 10.1021/acs.jmedchem.5b00911
J. Med. Chem. 2016, 59, 2381−2395

Table 1. continued

compd	sequence	K_i ± SD (nM)	ERK EC_{50} ± SD (nM)	cAMP EC_{50} ± SD (nM)	$T_{1/2}$ plasma
58	URRQ[CHA][ACC] -NH_2	12939 ± 4254			
59	Bz-PrrQ[CHA][MPC]C-NH_2	786 ± 389			
60	Bz-PrrQ[CHA]C[MPC] -NH_2	208 ± 68			
61	Nz-PrrQ[CHA]CC-*OH*	229 ± 19			30 min
62	4Cl-Bz-PrrQ[CHA]CC-*OH*	795 ± 135			
63	Bz-PrrQ[CHA]CC-*OH*	2141 ± 197			
64	Bz-PrrQ[CHA]-NH_2	22504 ± 3218			
65	Bz-PrrN[CHA]CC-NH_2	0.61 ± 0.12			
66	Bz-PrrR[CHA]CC-NH_2	0.23 ± 0.1			720 min
67	Bz-PrrK[CHA]CC-NH_2	0.59 ± 0.12			
68	Bz-PrrA[CHA]CC-NH_2	0.29 ± 0.14			
69	Bz-PrrL[CHA]CC-NH_2	1.4 ± 0.6			
70	Bz-PrrS[CHA]CC-NH_2	0.42 ± 0.11			
71	Bz-PrrF[CHA]CC-NH_2	0.59 ± 0.07			
72	Bz-PrrG[CHA]CC-NH_2	0.16 ± 0.03			60 min
73	Bz-PrrD[CHA]CC-NH_2	10.2 ± 2.1			
74	Bz-PrrE[CHA]CC-NH_2	19.4 ± 5.6			
75	Bz-Prr[CHA]CC-NH_2	60 ± 11.7			

[a]KOR binding affinity (K_i), selected functional data of key analogues (Surefire-ERK and cAMP, EC_{50}), and plasma half life ($T_{1/2}$) are shown. Data represented are the mean ± SD values from at least $N = 3$ experiments each performed in triplicate.

Table 2. Plasma Stability Evolution of Selected κ Agonist Peptides 23, 26, 39, 44, and 45[a]

compd	sequence	time of analysis [min]	fragments detected by MS	relative abundance by HPLC
23	URRQ[CHA]CC	60	URR	0.01
			Q[CHA]CC	0.01
			URRQ[CHA]	0.1
			URRQ[CHA]CC	1
26	UrrQ[CHA]CC	120	UrrQ[CHA]	0.1
			UrrQ[CHA]CC	1
39	BzPrrQ[CHA]CC	360	BzPrrQ[CHA]	0.1
			BzPrrQ[CHA]CC	1
44	UrrQ[CHA][PEN]C	3600	UrrQ[CHA][PEN]C	1
45	BzPrrQ[CHA][PEN]C	3600	BzPrrQ[CHA][PEN]C	1

[a]Formation of peptide fragments was investigated by analytical HPLC and mass spectroscopic characterization. On the basis of the fragments identified, the labile amide bonds were modified (**23** → **26** → **39** → **44** → **45**) to improve stability without adversely affecting KOR affinity (see Table 1).

evaluated by binding assays for KOR, MOR, DOR, and NOP to ensure selectivity for KOR with selected leads evaluated for KOR functional activity. GPCR signaling[56] is a very complicated process with multiple signaling pathways possible that are further complicated by crosstalk. KOR predominantly couples to $G_{i/o}$-proteins, which inhibit adenylate cyclases upon activation of the receptor which leads to an inhibition of cAMP production.[56] Two functional readouts[57] of KOR activation were chosen and monitored for this study: a cAMP assay[58] and an ERK1/2 phosphorylation assay.[59] The cAMP assay was selected as a measure of direct KOR mediated activation of $G_{i/o}$-proteins, and ERK1/2 assay was elected because it is further downstream of direct KOR activation and also encompasses signals generated by $G_{\beta/\gamma}$ subunits and β-arrestin activation of mitogen activated protein kinases (MAPK).[60]

Initial Structure–Activity and Metabolic Stability Profiling. An alanine scan of **1** resulted in analogues (**2**–**5**) and revealed that KOR affinity (Table 1) was reduced when residues 4–7 (RRQI) were individually replaced by alanine. The N-terminal asparagine (N) residue was replaced by a pyroglutamic acid (U) (→**6**) without affecting affinity, while an aromatic amino acid (Y) in this position improved affinity (→**7**). Truncation of peptide **1** (analogues **8**–**11**) revealed a minimal active sequence of RRQICC (**10**), with the C-terminal vicinal disulfide moiety identified as critical for high KOR affinity (→**8**, **9**). Vicinal disulfide moieties are found on active sites of enzymes,[61,62] near binding site on receptors,[61–63] and in a number of toxins.[64–67] In proteins, this unique eight-ring structure prefers to adopt a type VIII turn with a distorted trans-amide conformation.[61] In small peptides, cis or trans amide conformation is observed, with the strength of the disulfide bond increasing in the cisoid conformation.[68] The ability to ring system flip depending on redox state makes vicinal disulfide bonds an important class of regulatory conformational switches.[61,69] In small ring systems the vicinal disulfide bond has exceptional redox stability as well as structural importance.[18] Alanine scan analogues of **1** revealed that the Ile (I) positioned next to the vicinal disulfide also contributed to high affinity binding (**5**). To investigate this position further, analogues with aliphatic as well as aromatic residues were produced (**12**–**16**); these analogues indicated that binding affinity increased with the size of the aliphatic side chain (V, **12** < I, **1** < L, **13** < [CHA], **14**) (Table 1). Similar results were obtained with aromatic residues, with phenylalanine (F, analogue **15**) and naphthylalanine (**16**) replacements further enhancing KOR affinity (Table 1). Replacing the

DOI: 10.1021/acs.jmedchem.5b00911
J. Med. Chem. 2016, 59, 2381–2395

Table 3. Opioid Receptor Selectivity Data of Selected κ Agonist Peptides (1, 6, 11, 23, 26, 39, 44, and 45) Compared to Dynorphin A (1−17)[a]

compd	sequence	K_i ± SD (nM)	fold selectivity vs KOR		
			MOR	DOR	NOP
dynorphin A (1−17)	YGGFLRRIRPKLKWDNQ	0.28 ± 0.25	>60	>2000	>500
1 (1−2, 3−4)	NCCRRQICC	80.4 ± 42.6	>630	>630	>630
6	UCCRRQICC	67.5 ± 6.7	>630	>630	>630
11	URRQICC	191 ± 35	>250	>250	>250
23	URRQ[CHA]CC	6.7 ± 1.1	>10000	>10000	>10000
26	UrrQ[CHA]CC	3.9 ± 1.5	>10000	>10000	>10000
39	BzPrrQ[CHA]CC	0.25 ± 0.13	>250000	>250000	>45000
44	UrrQ[CHA][PEN]C	1.3 ± 0.5	>39000	>1200	>25000
48	BzPrrQ[CHG]CC	0.48 ± 0.22	>125000	>125000	>125000

[a]From the initial conopeptide hit (**1**), evolved molecules (**39**, **48**) show a clearly improved selectivity profile, while maintaining KOR affinity equipotent to dynorphin A.

strongly basic arginine (R) residues with histidine (H) (**17**, **18**), lysine (K) (**19**, **20**), or citrulline [CIT] (**21**, **22**) decreased binding affinity, suggesting that arginine is optimal at this position for KOR affinity. Combining these favored replacements generated URRQ[CHA]CC (**23**), which had a 10-fold improved binding affinity compared to **1** at KOR; thus **23** was chosen as a promising early lead.

Peptides **1** and **23** survived intact for only a few minutes in plasma and therefore were not considered suitable for further development (Table 2 and Figure 3). From stability studies of **23** in rat plasma (Table 2), it was found that the main cleavage site was at the vicinal Arg, as well as a minor cleavage site between [CHA]-5 and the vicinal disulfide moiety. However, reduction of the vicinal disulfide bond was not observed in any of the peptides investigated, confirming its previously observed redox stability.[18] The major site of metabolic liability was addressed by the introduction of D-Arg residues (**24**−**26**) that maintained binding affinity to KOR but had significantly increased plasma stability, with UrrQ[CHA]CC (**26**) showing a plasma half life of 6 h (Table 1). Table 2 shows the absence of fragments related to cleavage within the Arg region of **26**, confirming that the L- to D-Arg change directly enhanced metabolically stability.

Design of Improved KOR Agonists. From initial analog design, YCCRRQICC (**7**) had slightly improved binding affinity compared to **1**, indicating additional aromatic participation might further improve binding affinity at KOR as observed for dynA (1−17) and other enkephalins.[44] From this knowledge and the sequence similarity of our KOR agonist peptides like **7** with dynA (1−8), we designed analog **26** with an aromatic substituted N-terminus. Further analogs included N-terminal capping using aryl substituted acetic (**27**−**29**) or propanoic acid (**30**−**32**), bicyclic aromatic and heteroaromatic building blocks (**33**−**36**), and substitution of the pyroglutamyl moiety with proline and subsequent N-benzoylation (**37**−**43**) (see Figure 2). As expected, a number of these N-terminal analogues had enhanced affinity (Table 1). Whereas benzoyl substitutions (**27**−**29**) appeared unable to access the aryl-binding pocket of the receptor, the CH_2 extended benzyl-carboxyl substituents (**30**−**32**) enhanced affinity and the more constrained bicyclic analogues (**33**−**36**) yielding further improvements in affinity. Subnanomolar affinity analogues (**37**−**43**) were produced by substituting the pyroglutamate residue in **26** with the structurally related proline in combination with *N*-benzoyl aromatic substitution (Table 1).

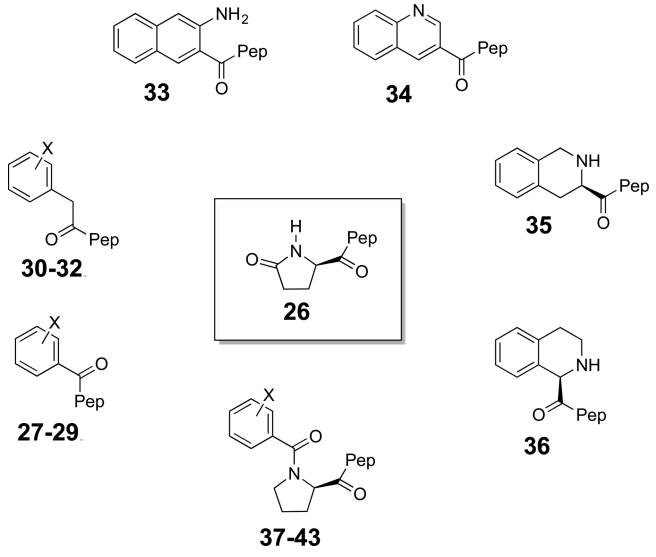

Figure 2. N-terminal aryl modifications of **26** (UrrQ[CHA]CC-NH_2. Substitution of the pyroglutamate (U) residues by aryl substituted building blocks resulted in significantly improved KOR agonist (**30** → **43**). Pep = peptidyl residue with sequence *HN*-rrQ[CHA]CC; X = aryl substituent. For sequence details and KOR binding see Table 1.

Enhancing High Affinity KOR Agonist Stability. Peptide **26** and high affinity analogues **33**−**43** were unstable in plasma (Table 2 and Figure 3), with prominent cleavage evident between the amide bond of the cyclohexylalanine [CHA] residue and the vicinal disulfide bond. Introducing a penicillamine [PEN] at Cys6, adjacent to the labile amide bond,

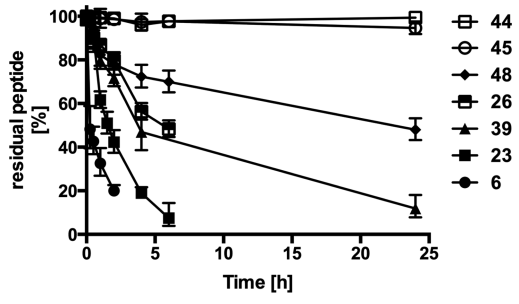

Figure 3. Plasma stability conorphins **6**, **23**, **26**, **39**, **44**, **45**, and **48** in rat plasma at 37 °C. Shown is % remaining peptide determined by HPLC over time.

DOI: 10.1021/acs.jmedchem.5b00911
J. Med. Chem. 2016, 59, 2381−2395

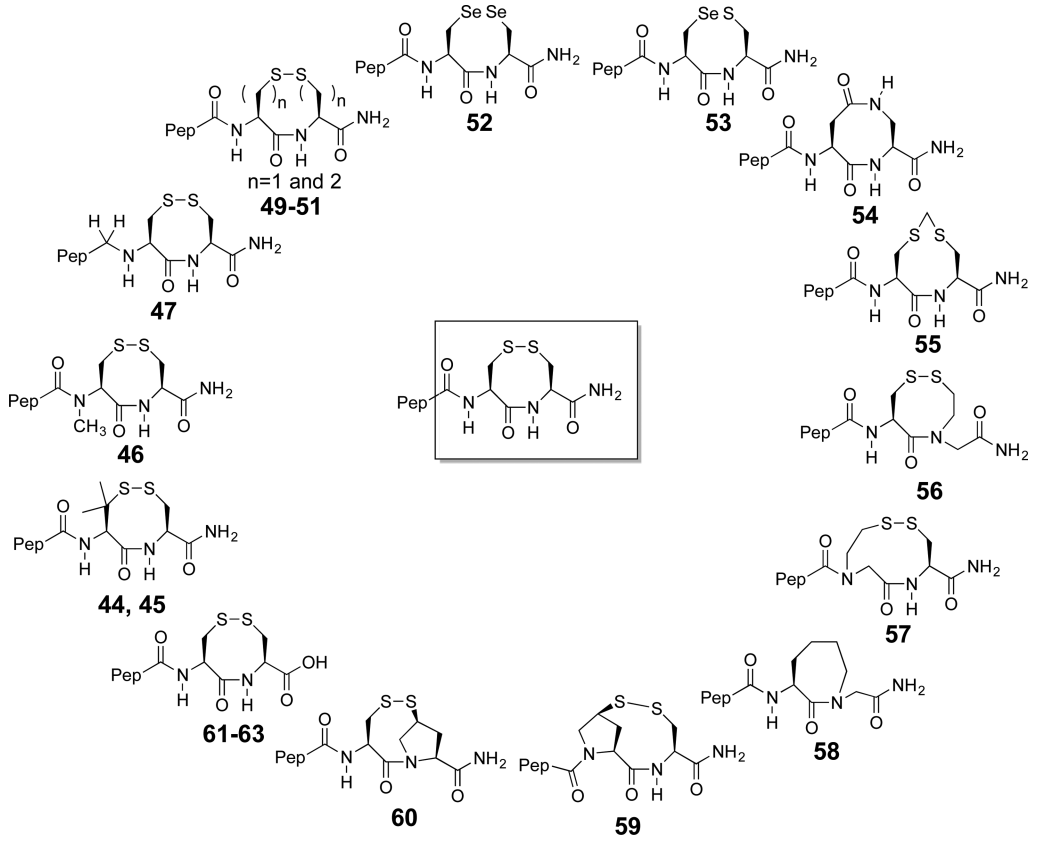

Figure 4. Vicinal disulfide mimetics. Modifications of C-terminal vicinal disulfide moiety and adjacent amide bonds (structure shown in square) in peptides **44**–**63**. Pep = peptidyl residue XrrQ[CHA] with a N-terminal modification X as shown in Table 1.

significantly improved plasma stability (see **44**, **45** in Table 2 and Figure 4) most likely by the two protruding β-methylene groups of PEN restricting protease access. The introduction of penicillamine into the vicinal disulfide bond (**26** → **44**) maintained binding affinity, though the benzoyl-prolyl analogue **39** lost affinity at KOR after introduction of the PEN residue (**39** → **45**). This affinity shift further confirmed the importance of the vicinal disulfide as part of the pharmacophore for this class of peptides and suggested that this moiety may structurally preorganize the pharmacophore to enhance KOR affinity.

To stabilize the labile amide bond, we N-methylated Cys6 of **39** (**39** → **46**) by site directed N-methylation via sulfonamide formation, using a Mitsunobu reaction with methanol and final removal of the activating sulfonamide by adapting a procedure from Biron et al.[70] However, the *N*-methyl analogue **46** had reduced KOR affinity. Reduction of the amide bond in **39** via an adaptation to the procedure of Guichard et al.,[71] where the amide carbonyl (C═O) group was replaced with a CH_2 group to yield a methylene–amino (CH_2–NH) linkage from the CHA-5 residue to the Cys-6 residue **47**, resulted in a 4-fold plasma half-life improvement ($t_{1/2}$ = 16 h) but reduced KOR affinity compared to **39**. The methylamino group introduction in **47** was achieved using Fmoc-cyclohexylalanine, transfer to its Weinreb amide, cyanoboron hydride reduction to the respective amino acid aldehyde, and final reductive amination on solid phase onto a H_2N–CC Rink amide resin using an adaptation to a procedure by Guichard et al.[71] Further stability improvements were achieved by replacing the CHA-5 residue with a cyclohexylglycine [CHG] (**39** → **48**), and **48** maintained KOR affinity, with an improvement in plasma stability to $t_{1/2}$ = 20 h.

Vicinal Disulfide Ring Mimetics. To investigate the role of the vicinal C-terminal cysteine moiety, we introduced a number of eight-membered ring mimetics (Figure 4). Replacement of cysteine by homocysteine either individually or together yielded analogues with extended ring sizes (**49**, **50**) resulting in a significant loss of KOR affinity. Replacement of the disulfide bond by a diseleno bond (**35** → **52**) or a sulfur-seleno bond (**26** → **53**) was possible without loss of affinity, but no metabolic stability improvement was observed. The replacement of the disulfide bond with an amide bond (**54**) was achieved via side chain to side chain cyclative amidation between an aspartic acid and α,β-diaminopropionic residue, yielding a cyclic product with the same ring size as the vicinal cysteine (**54**); however, this analogue showed a significant loss of KOR affinity. An increased ring size that maintained the soft polarizable sulfur atoms within the ring system was obtained by inserting a methylene bridge (-S-CH_2-S-) to generate the methylene dithioether peptide **55** using a solid phase adaptation from Ueki et al.[72] However, the resultant dithiomethylen ether derivative **55** also showed reduced KOR affinity. The ring size was also varied by incorporation of *N*-thiomethylglycine building blocks instead of cysteine resulting in a seven- (**56**) or nine-member (**57**) ring system containing both a disulfide bond and an N-substituted amide bond. Both analogues lost KOR affinity, and replacement of the S–S bond in compound **56** by a CH_2–CH_2 in **58** almost abolished KOR affinity. To incorporate an additional constraint into the vicinal C-terminal moiety, 4-thioproline building blocks were used to generate bicyclic products (**59**, **60**) that also lost KOR affinity. Finally, we investigated the role of the C-terminal amide. Synthesis of the most active KOR agonists (**37**–**39**) as the acid

DOI: 10.1021/acs.jmedchem.5b00911
J. Med. Chem. 2016, 59, 2381–2395

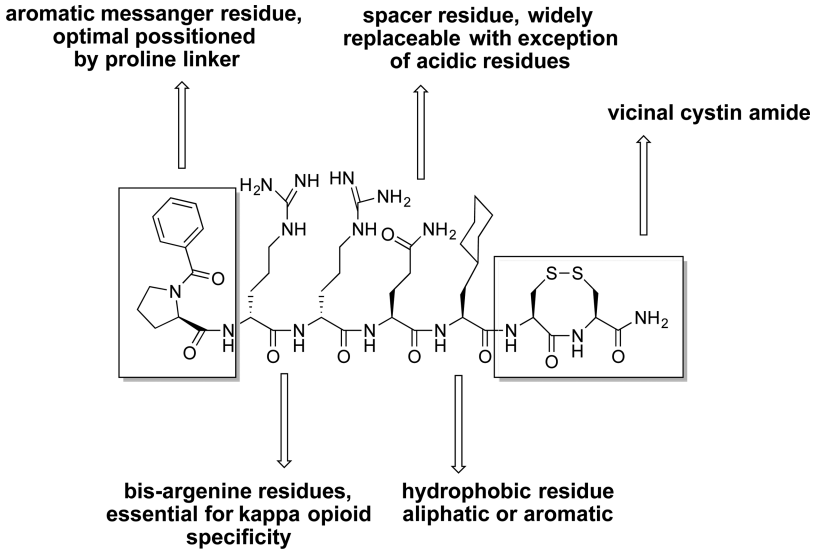

Figure 5. KOR pharmacophore model for conorphins built from **39**.

form (**61**−**63**) produced peptides with greatly reduced affinity for KOR.

Although we were able to replace the vicinal disulfide with a wide variety of structural mutations, most of these analogs had reduced affinity for KOR. This suggested that the eight-membered vicinal cysteine ring system is a critical component of the pharmacophore for this series of KOR receptor agonists, perhaps through a structural preorganization or because the disulfide-containing moiety interacts with the KOR. If the role of the vicinal disulfide moiety were purely structural, replacing the vicinal disulfide bond with bioisosteric groups that mimic the vicinal disulfide moiety would be expected to have little effect on KOR activity. Selenium has very similar physicochemical properties as sulfur,[73] and it has been shown that diseleno and seleno-sulfur bridges can be used to replace disulfide bridges without affecting structure.[74] The synthesized selenocysteine analogues **52** and **53** had similar KOR affinity compared to their disulfide analogues **26**−**35**, supporting the importance of the vicinal disulfide moiety as a structural contributor of the pharmacophore. This is further confirmed; when peptide **39** is truncated and the vicinal cysteine removed, the remaining hexapeptide **64** is completely inactive at KOR.

Role of the Gln Insert in Conorphins. From previous chimeric peptide studies[45,46] it is suggested that dynA (6−8) (Arg6-Arg7-Ile8) contributes to the selectivity for KOR whereas our series contains Arg-Arg-Gln-Ile. To investigate the role of the glutamine (Gln, Q) inserted between the arginine residues and the aliphatic isoleucine/cyclohexylalanine residues, several analogues were produced replacing glutamine (**65**−**74**). The majority of amino acids were well tolerated (**65**−**72**) with the exception of aspartic and glutamic acid (**73**, **74**), which lost significant KOR affinity (Table 1). Surprisingly, deleting the glutamine residue from the sequence (**75**) also strongly reduced binding affinity to KOR. These results indicate that glutamine is not part of the pharmacophore but acts as spacer for optimal presentation of the conorphin pharmacophore. Consistent with this conclusion, replacing glutamine with a glycine residue (**72**) had little effect on KOR affinity.

Functional Assay of Developed Conorphines. The conorphin SAR and pharmacophore development was driven by affinity data obtained from a radioligand binding assay. To further validate select key molecules **1**, **6**, **11**, **23** **26**, **39**, **44**, and **48**, we performed functional assays[57] monitoring the efficacy of these ligands on two key intracellular signaling pathways, namely, cAMP[58] for direct KOR activation and ERK1/2[59] as a pathway further downstream of $G_{i/o}$-protein activation and encompassing contributions from $G_{\beta/\gamma}$-subunits and β-arrestins. These functional assays delivered efficacy data (Table 1) that confirmed the molecules as full agonists at KOR (intrinsic efficacies of molecules **1**, **6**, **11**, **23**, **26**, **39**, **44**, and **48** compared to dynA (1−17) were all in the range of 90−150%; see Supporting Information comparing initial lead molecule **1** and advanced analogue **39** with dynA (1−17)). Interestingly, the most potent analogues **39** and **48** had similar affinity and efficacy (cAMP and ERK1/2) at KOR as dynA (1−17) (Table 1). Less potent analogues **1**, **6**, **11**, **23**, **26**, and **44** showed some discrepancies between binding affinity and the efficacy measured at the two functional assays. The biased signaling of molecules is currently of great interest in the field of pharmacology, as it has been suggested that biased ligands maybe able to avoid the side effects associated with some drugs that activate all pathways of a receptor equally.[75] These data provide a basis for future detailed studies into the biased signaling nature of some molecules, which is already of interest for the opioid receptors as a possible mechanism to avoid side effects.[76]

Selectivity Profile of Developed Conorphins. The previously described lead optimization work was strongly focused on KOR affinity and peptide stability optimization. To ensure that while improving activity, selectivity for KOR was not lost, we investigated selected key milestone molecules (**1**, **6**, **23**, **26**, **39**, **44**, **48**), where strong structural changes were made, for their receptor selectivity. The selectivity profile of dynA (1−17) and selected peptides, e.g., **1**, **6**, **23**, **26**, **39**, **44**, **48** at other opiate receptors (Table 3) indicated that improvements in KOR affinity paralleled improvements in KOR selectivity relative to MOR, DOR, and NOP.

Conorphin Pharmacophore Model. The pharmacophore of this novel series of KOR agonist peptides[33] is represented using the most potent analogue **39** in Figure 5. The pharmacophore is defined by an aromatic N-terminal residue

DOI: 10.1021/acs.jmedchem.5b00911
J. Med. Chem. 2016, 59, 2381−2395

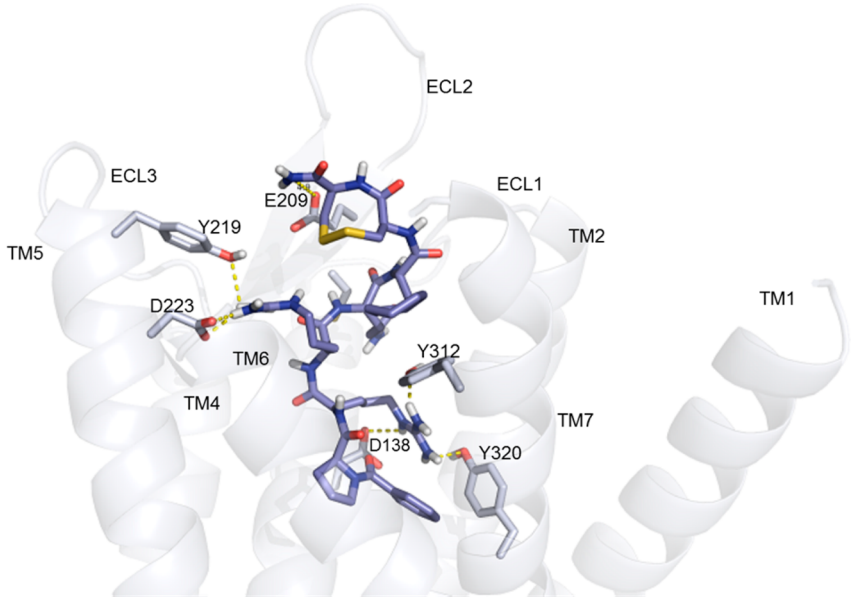

Figure 6. Energy minimized docked pose of the KOR agonist **39** with the KOR. The key interactions are identified, with the carboxyl group of the benzoyl residue forming a strong hydrogen bond with Asp138 positioning the aromatic benzoyl moiety to form hydrophobic interactions with residues lining the TMIII. The guanyl-NH of Arg3 in **39** forms strong H-bond interactions with Tyr312 and Tyr320 in TMH7. Arg4 was rotated in the opposite direction forming a salt bridge with Asp223 in TMH5 and a H-bond with Tyr219 in TM5. The amide bond between Arg4 and Gln5 of peptide ligand **39** forms strong hydrogen bonds with Ser211 and Cys210 in ECL2 which provides a binding conformation specific to this peptide. The hydrophobic amino acid in position 5 [CHA] leads to a gain of activity due to hydrophobic interaction with residues lining TMH7, including a strong interaction with Tyr312. The C-terminal amide of the peptide ligand **39** and Glu209 form a characteristic H-bond interaction with the vicinal disulfide moiety of importance for the placement of the C-terminal amide function. The vicinal disulfide moiety itself also forms strong hydrophobic interaction with the cyclohexyl residue of **39** and weak van der Waals and hydrophobic interactions between the vicinal disulfide eight-membered ring moiety and residues at the extracellular part of the TM3, TM4, TM5.

Table 4. Prominent Interactions of the KOR Receptor Residues with DynA (1−8) and KOR Agonist 39 Reveal a Strong Binding Site Overlap[a]

KOR receptor	dynA (1−8)	peptide ligand **39**
Asp138 (TMIII)	**NH_2**-Tyr1/Tyr1-**CO**-**NH**-Gly2	Bz-**CO**-
Cys210		Arg4-**CO**-**NH**-Gln3
Ser211	Arg6-**CO**/Arg-6-**guanyl**	Arg4-**CO**-**NH**-Gln3
Tyr219	Arg7-**guanyl**	Arg4-**guanyl**
Asp223	**HO**-Tyr1	Arg4-**guanyl**
Tyr312	Gly3-**CO**-NH-Phe4	Arg3-**guanyl**
	Phe4-CO-**NH**-Ile5	
	Ile5-**CO**-NH-Arg6	
	Arg7-**CO**-NH-Ile8	
Tyr320		Arg3-**guanyl**

[a]Interacting sites on the ligands are shown in bold.

[BzoP-1] where proline acts as spacer and structural constraint, with the aromatic moiety amidating proline's nitrogen atom. We showed that the subsequent arginine residues (Arg2, Arg3) are essential for high KOR affinity, with D-Arg replacements producing potent analogues with improved plasma stability. The glutamine residue (Gln-4) appears to act as a simple spacer group to the adjacent position [CHA]-5, which was critical for high affinity binding. While cyclohexylalanine [CHA] showed the best results, other aliphatic and aromatic residues are accepted at this position, indicating an interaction with a hydrophobic binding pocket within KOR. The C-terminal vicinal disulfide cysteine pair was essential in maintaining high KOR affinity, and most alterations significantly reduced KOR affinity. The C-terminal amide also contributes to KOR affinity, indicating that the vicinal disulfide might play a spacer role to influence the relative orientation of the C-terminal amide and the rest of the pharmacophore, as well as potentially having structurally stabilizing and/or direct interactions with the KOR receptor. Unfortunately, NMR investigation of compound **39** showed multiple conformations in solution, making an exact structure model unfeasible. On the basis of the SAR evidence provided, we conclude that these KOR agonists might mimic the interaction of dynA with the KOR. To strengthen this conclusion, based on the obtained SAR data, a docking study of the peptide ligand **39** to the orthosteric binding site of the KOR was performed with AutoDock, and was confirmed against the docking results obtained for dynA (1−8).[50]

Molecular Docking of 39 and dynA (1−8) to KOR. To validate our docking simulations, dynA (1−8) was docked (AutoDock) to a model of the KOR built from an X-ray structure of KOR in complex with a small molecule antagonist (JDTic).[49] The obtained lowest energy binding pose was

DOI: 10.1021/acs.jmedchem.5b00911
J. Med. Chem. 2016, 59, 2381−2395

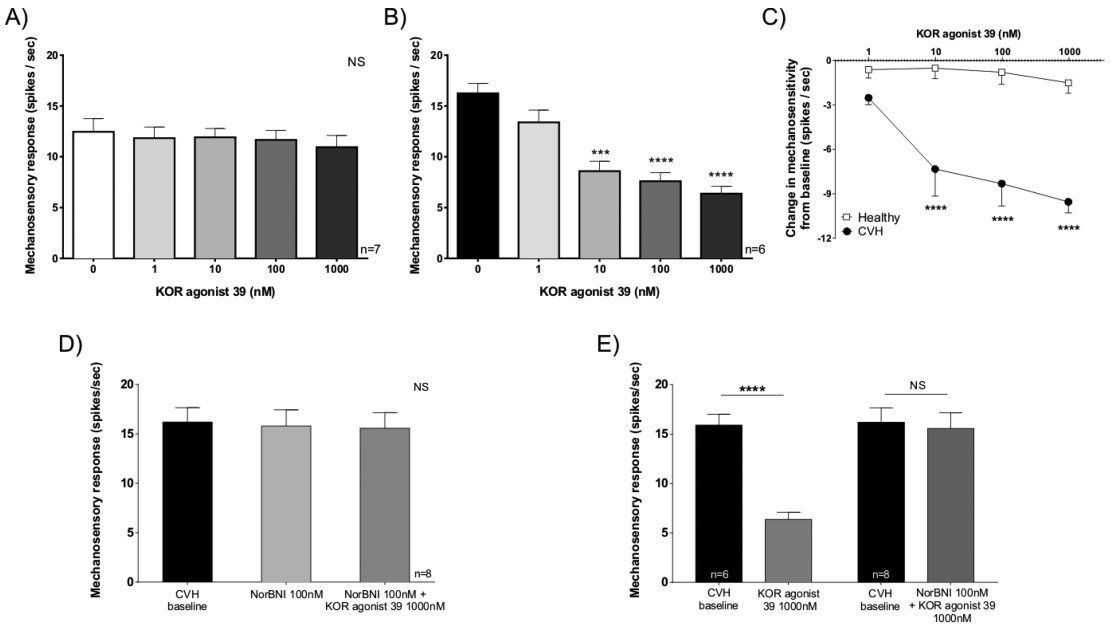

Figure 7. (A) The KOR agonist **39** had no effect on healthy splanchnic colonic nociceptor mechanosensitivity at any of the doses tested ($P > 0.05$, $n = 7$). (B) However, the KOR agonist **39** caused dose-dependent inhibition of colonic nociceptors from mice with CVH (28-days post-TNBS administration; (***) $P < 0.001$ at 10 nM; (****) $P < 0.0001$ at 100 nM and 1000 nM, $n = 6$; one-way ANOVA, Bonferroni post hoc). (C) Change in mechanosensitivity induced by the KOR agonist **39** in healthy and CVH nociceptors compared to their respective baselines. The KOR agonist caused significantly more inhibition at 10 nM ((****) $P < 0.0001$), 100 nM ((****) $P < 0.0001$), and 1000 nM ((****) $P < 0.0001$) in CVH nociceptors than healthy nociceptors (two-way ANOVA, Bonferroni post hoc). (D) This KOR agonist **39** induced inhibition of CVH nociceptors was blocked by prior addition of the KOR antagonist Nor-BNI (100 nM; $P > 0.05$, $n = 8$), confirming the involvement of KOR activation in the observed effect. (E) A single dose of KOR agonist **39** (100 nM) inhibited CVH colonic nociceptor mechanosensitivity ((****) $P < 0.0001$, $n = 8$). Comparison of the inhibitory effect of the KOR agonist **39** ($n = 8$) vs Nor-BNI plus KOR agonist **39** ($n = 8$) shows that the inhibitory effect of KOR agonist **39** is blocked by the KOR antagonist.

compared to the pose previously generated for dynA (1−8).[50] Consistent with this docking pose, strong H-bonds are formed between the N-terminal amine and Asp138, a hydrogen bond was also observed between the NH of the amide bond between Tyr1 and Gly2 of dynA (1−8) and Asp138 in the receptor, and Gly2 and Gly3 are at the base of the orthosteric binding site. In this pose, the CO between Gly3 and Phe4, the NH between Phe4 and Ile5, the CO between Ile5 and Arg6, and the CO between Arg7 and Ile8 form hydrogen bonds with Tyr312 in TMH7, Tyr1-hydroxyl forms weak interactions with Lys227 and Asp223 in TMH5, Phe4 forms hydrophobic interactions with residues lining the TMH3, and Asp138 in TMH3 forms a strong hydrogen bond with the amide bond between Phe4 and Ile5. This pose allows the two arginine to face toward TMH5 and ECL2, with Arg6 interacting with Ser211 in ECL2 and Arg7 with Tyr219 in TMH5 via hydrogen bonds and the terminal amide of dynA (1−8) to interact with Tyr313 in TMH7 and Gln115 in TMH2. These interactions of dynA (1−8) with KOR are consistent with the results[50] previously described, validating our docking studies.

By use of the same approach, the molecular docking of KOR agonist **39** (see Figure 6) revealed a low energy docking pose that partially overlapped the binding site with dynA (1−8) and was consistent with our structure−activity studies (see Table 4). Similar to what was observed for dynA (1−8) is Asp138 in TMH3 strongly involved in binding of **39**. Rather than the observed salt bridge between the N-terminal amine and Asp138 in the dynA (1−8) docking pose, we did observe that the carboxyl group of the benzoyl residue in **39** forms a strong hydrogen bond with Asp138 in TMH3 in the orthosteric binding site, while the aromatic benzoyl moiety forms hydrophobic interactions with residues lining the TMIII. The benzoyl-prolyl residue in the orthosteric site is further stabilized by the interaction of NH between Arg3 with Tyr312 in TMH7, while the guanyl-NH of Arg3 in **39** formed strong H-bond interactions with Tyr312 and Tyr320 in TMH7. The lowest energy binding pose revealed Arg4 was rotated by 180° compared to dynA (1−8) to form a strong salt bridge with Asp223 in TMH5 and a H-bond with Ser211 in ECL2. These strong Arg3 and -4 interactions are consistent with these arginine residues being essential for high affinity binding to the KOR. The amide bond between Arg4 and Gln5 of peptide ligand **39** forms strong hydrogen bonds with Ser211 and Cys210 in ECL2 which provides an ECS (extracellular surface) binding conformation specific to this peptide. Gln5 in **39** holds minor interactions with the receptor residues surrounding TMII and TMIII, which explains our SAR results, that many Gln5 amino acid substitutions are tolerated (e.g., **65**−**71**) without loss of activity. In contrast, acidic groups in position 5 resulted in strong activity loss (e.g., **72**, **73**). We speculate that this is due to the presence of the acidic residues in the upper half of the ECS imparting negative charge to the receptor, thereby repelling most of the acidic peptide ligands (e.g., **72**, **73**, and **61**−**63**) attempting to enter the orthosteric binding site. The in position 6 located cyclohexyl alanine residue is important for high KOR affinity. A change in size of the hydrophobic side chain has resulted in gain of activity (see **12**; V < **13**; L < **14**; [CHA]), but also aromatic residues such as Phe (**15**) or [NAL] (**16**) are tolerated at this position. The observed docking model reveals hydrophobic interaction with residues lining TMH7 (Leu309, Tyr313), including a strong interaction with Tyr312. Furthermore, a close proximity (4.4

DOI: 10.1021/acs.jmedchem.5b00911
J. Med. Chem. 2016, 59, 2381−2395

Å) of the disulfide bond in **39** and the cyclohexyl residue was observed which is indicative for intramolecular hydrophobic interaction resulting in structural constraining of **39** within the KOR binding site. This intramolecular interaction may explain the importance of the vicinal disulfide bond in the observed SAR studies. A characteristic weak hydrogen bond is observed between the C-terminal amide of the peptide ligand **39** and Glu209 after energy minimization of the docked structure with YASARA Web server. The activity loss for the C-terminal acid version (**61**−**63**) of peptide agonist can again be explained by the unfavorable repulsion with Glu209 and with the highly acidic extracellular surface limiting access to the orthosteric site. The vicinal disulfide moiety adjacent to the C-terminal amide is important for the placement of the C-terminal amide function. But the vicinal disulfide moiety itself also forms strong intramolecular hydrophobic interaction with the cyclohexyl residue in **39** and is not well-defined at the mouth of KOR with weak van der Waals and hydrophobic interactions between the vicinal disulfide eight-membered ring moiety and residues at the extracellular part of the TMIII, TMIV, TMV, TMVI, and TMVII. This observed intramolecular hydrophobic interaction between the disulfide bond and cyclohexyl alanine as well as the H-bond between the C-terminal amide and Glu209 may explain the importance of the vicinal disulfide group for maintaining of bioactivity and herewith the detrimental effect if replaced by any other moiety (see **54**−**60**) or deleted from the molecule (→**64**). As a caveat of these interpretations, one should keep in mind that the employed KOR model was based on an X-ray structure in an antagonist bound conformation.[49]

Nevertheless the obtained docking pose of the peptide agonist **39** shown in Figure 5 can explain the obtained SAR results to a large extent and does herewith also confirm the proposed SAR based pharmacophore model. Therefore, we have shown that the developed KOR agonists of type **39** are peptide mimetics of dynorphin A.

Analgesic Action of 39 in a Model of Chronic Visceral Hypersensitivity (CVH). We have previously established that KOR expression on colonic nociceptors is functionally up-regulated during chronic visceral hypersensitivity (CVH) associated with chronic abdominal pain.[43] Analogue **39** was tested for the ability to modify colonic nociceptor mechanosensory function in healthy and during postinflammatory chronic visceral mechanical hypersensitivity (CVH). Compound **39** was tested on the mechanosensitivity of colonic afferents using ex vivo recordings of mice splanchnic high-threshold afferents. These afferents respond to focal compression and have response thresholds above the physical range and thus likely function as nociceptors. Additionally, they display pronounced mechanical hypersensitivity and lowered activation thresholds in models of acute and chronic visceral pain. Nociceptor mechanosensitivity was assessed before and after increasing doses of **39**. Agonist **39** had no effect at any dose tested on healthy nociceptor mechanosensitivity (Figure 7A). In contrast, when recordings were performed from mice with CVH, **39** showed dose-dependent inhibition of colonic nociceptor mechanosensitivity (Figure 7B). Overall, **39** had a significantly greater inhibitory effect in the CVH model (Figure 7C). On the basis of these results, it can be concluded that **39** inhibits splanchnic colonic nociceptor mechanosensitivity during CVH but not in normal healthy colon. We also show that the inhibitory effect of **39** is blocked by a KOR selective antagonist (nor-BNI; norbinaltorphimine) (Figure 7D and Figure 7E). The select inhibitory effect of KOR agonist **39** is consistent with our previous findings using asimadoline, which only showed efficacy in the CVH state[43] and appears to inhibit nociception via activation of KORs expressed on the peripheral endings of colonic nociceptors, suggesting a peripherally restricted KOR agonist might be useful treatment for a variety of visceral pain conditions including irritable bowel syndrome. Notably, in human patients with IBS, asimadoline has been shown to significantly decrease pain perception in response to colonic distension.[77] Interestingly, in a phase IIb study asimadoline's efficacy against symptoms of IBS was greatest in D-IBS patients, with at least moderate pain at baseline.[78]

CONCLUSION

A first of a kind class of KOR agonists were discovered and developed based on the initial nine-residue hit from a conopeptide venom library. Through systematic structure−activity relationship (SAR) elaboration, conorphin-T led to the development of an initial pharmacophore containing a critical C-terminal vicinal disulfide that allowed for the rational design of analogues with highly improved properties. The initial lead **1**, which had a short plasma half-life ($t_{1/2}$ = 15 min) and nanomolar affinity and micromolar efficacy (K_i = 80.4 nM, EC_{50} = 9.848 μM), was systematically modified to yield eight-residue peptides (e.g., **39**) with subnanomolar affinity, efficacy (K_i = 0.25 nM, EC_{50} = 0.36 nM) and improved plasma stability ($t_{1/2}$ = 240 min). Using in vitro metabolic studies, we were able to identify cleavage sites that were modified to produce analogues with significantly improved plasma stability (>24 h). These stable, potent, and selective KOR agonists contained a pharmacophore resembling that of dynorphin A, with modeling studies revealing dynA (1−8) and **39** to have overlapping binding sites on KOR. The KOR agonist **39** inhibited splanchnic colonic nociceptors during CVH but not in the normal healthy colon and represents promising a lead for the development of IBS treatments.

EXPERIMENTAL SECTION

Materials. Protected Fmoc-amino acid derivatives were purchased from Novabiochem or Auspep P/L. The following side chain protected amino acids were used: Cys(Acm), Cys(Trt), His(Trt), Hyp(tBu), Tyr(tBu), Lys(Boc), Trp(Boc), Arg(Pbf), Asn(Trt), Asp(OtBu), Glu(OtBu), Gln(Trt), Ser(tBu), Thr(tBu), Tyr(tBu). All other Fmoc amino acids were unprotected. Unusual Fmoc amino acids [HTY], [ORN], [HLY], [CIT], and [BHK] were used with following side chain protections: -OH as -O^{t}Bu, -NH_2 as -NH(Boc), -COOH as -COO(^{t}Bu), and -SH as -S(Trt). All other unusual Fmoc amino acids were used unprotected. Unusual amino acids were sourced from Novabiochem, Auspep, CSPS-Pharmaceuticals, or NeoMPS. L-α-Hydroxyisovaleric acid was used unprotected. Dimethylformamide (DMF), dichloromethane (DCM), diisopropylethylamine (DIEA), trifluoroacetic acid (TFA) were supplied by Auspep P/L (Melbourne, Australia) as peptide synthesis grade. 2-(1*H*-Benzotriazol-1-yl)-1,1,3,3-tetramethyluronium hexafluorophosphate (HBTU), triisopropylsilane (TIPS), Tris-HCl, $MgCl_2$, bovine serum albumin (BSA), HEPES, EDTA, glycerol, HPLC grade acetonitrile, and methanol were supplied by Sigma-Aldrich (St. Louis, MO, USA). The resin used was Fmoc-Rink resin (0.65 mmol/g) supplied by Auspep P/L, and Wang resin (0.81 mmol/g) was supplied by Novabiochem. Ethane dithiol (EDT) was supplied by Merck, ^{3}H-U69,593, ^{3}H-naltrindole, ^{3}H-diprenorphine, ^{3}H-nociceptin, DOR, MOR, NOP membranes, FlashBlue GPCR scintillation beads, Alphascreen SureFire phospho-ERK1/2 kit were purchased from PerkinElmer (Waltham, MA, USA). Trans-IT CHO transfection kit was purchased from Mirus (Madison, WI, USA). Ham's F-12 media,

DOI: 10.1021/acs.jmedchem.5b00911
J. Med. Chem. 2016, 59, 2381−2395

FBS, trypsin-EDTA, and PBS were purchased from Life Technologies (Carlsbad, USA).

Synthetic Strategy. Peptide amides were synthesized on an Advanced ChemTech (ACT-396) automated peptide synthesizer using Rink amide resin (0.05 mmol). Peptide acids were synthesized on Wang resin loaded with the C-terminal Fmoc-Cys(Trt)-*OH* using MSNT/1-methylimidazole activation (4 equiv excess). Continued assembly for the peptide acids as well as the complete assembly of peptide amides was performed using HBTU in situ activation protocols[79] to couple the Fmoc-protected amino acid or unprotected acids to the resin (4 equiv excess). After chain assembly and, if required, final Fmoc deprotection, the reaction block was transferred onto an ACT-LABTECH shaker and peptides were cleaved from the resin at room temperature (rt) in TFA:H_2O/TIPS/EDT (87.5:5:5:2.5) for 3 h. Cold diethyl ether (30 mL) was then added to the filtered cleavage mixture and the peptide precipitated. The precipitate was collected by centrifugation and subsequently washed with further cold diethyl ether to remove scavengers. The final product was dissolved in 50% aqueous acetonitrile and lyophilized to yield a white solid. The crude, reduced peptide was examined by reversed-phase HPLC for purity and the correct molecular weight confirmed by electrospray mass spectrometry (ESMS).

Synthesis of *N*-Methylcysteine Containing Peptide 46. Peptide **46** was assembled using the above standard Fmoc protocol (0.1 mmol Rink amide resin) with the following exception; after coupling of the second cysteine to the resin and Fmoc deprotection, N-methylation was performed on resin.[70] An *o*-nitrobenzoylsulfonamide is introduced using 66 mg of *o*-nitrobenzenesulfonyl chloride and 66 μL of 2,4,6-collidine in 1 mL of dichloromethane (18 h, 25 °C). After washing multiple times with dichloromethane and dry tetrahydrofuran the acidified sulfonamide N-H was methylated with methanol (20 μL) at rt for 18 h in 2 mL of THF using 131 mg of triphenylphosphine and 300 μL of diisopropyl azodicarboxylate. After washing with THF and DCM the sulfon group was removed with 100 μL of DBU and 100 μL of 2-thioethanol in 1 mL of DCM. After washing of the resin with DCM and DMF the next amino acid was coupled using a double coupling performed with HBTU activation. Peptide **46** was then further assembled using the above-described standard synthesis procedure followed by cleavage and oxidation.

Synthesis of Reduced Amide Bond Peptide 47. Peptide **47** was assembled using the above standard Fmoc protocol on a Rink amide resin (0.4 mmol) coupling the first two cysteines and deprotecting the N-terminal Fmoc-protecting group. The reduced amide bond was formed by reductive amidation employing initial immin formation for 1 h with Fmoc-cycloheylalaninealdehyde (1.8 mmol) in NMP (10 mL) containing 1% acetic acid. This step was followed by immin reduction for 48 h using Na(CN)BH_3 (20 mmol) in NMP containing 1% acetic acid. The resin was washed multiple times with DMF (1% HOAc), MeOH, DCM, and DMF, and the synthesis was continued using standard Fmoc protocol. The Fmoc-cyclohexylalaninealdehyde[71] was synthesized from Fmoc-cyclohexylalanine (3.53 mmol) and coupling of *N*,*O*-dimethylhydroxylamine hydrochloride (3.6 mmol) in DCM using BOP (3.53 mmol)/DIEA (10 mmol) activation to form the amino acid Weinreb amide. After dilution with 200 mL of DCM the solution was extracted with solutions of $NaHCO_3$, HCl, $NaHCO_3$, and water. The organic phase was dried with $MgSO_4$ and the solvent was evaporated to deliver 1.3 g (85% yield) of crude Fmoc-cyclohexylalanine Weinreb amide. The Weinreb amide (2.97 mmol) was dissolved in 25 mL of dry THF and cooled to −20 °C. $LiAlH_4$ (3.6 mmol) was added in portions, and the mixture was stirred until 0 °C was reached. This temperature was maintained for a further hour. For workup, 100 mg of citric acid and ice was slowly added to the reaction mixture. After extraction with DCM and drying of the organic phase with $MgSO_4$ the solvent was removed to deliver 760 mg (2 mmol, 68% yield) of crude Fmoc-cyclohexylaldehyde as confirmed by LC−MS and was used without further purification in reductive amidation described above.

Synthesis of Side Chain to Side Chain Amidated Peptide 54. Peptide **54** was assembled under standard conditions as described above. After HPLC purification of the linear peptide Bz-PrrQD[DAP], side chain to side chain cyclization was obtained by dissolving 27 mg of starting peptide in 30 mL of DMF and adding 1 mL of a 0.05 M BOP solution in DMF and 1 mL of DIEA. Reaction monitoring employing HPLC−MS was indicating completion of cyclization within 1 h. The reaction solution was diluted with 200 mL of water (0.05% TFA) and loaded onto a C18 HPLC column for immediate purification.

Synthesis of Methylene Dithioether Peptide 55. On Rink amide resin (50 mg) the C-terminal dual cysteine sequence was assembled using standard HBTU activation. The cysteine building blocks used were side chain S-protected with the acid labile *p*-methoxytrityl group. After Fmoc deprotection the CC-Rink resin was S-deprotected using 2% TFA/4% TIPS in DCM (6 × 2 min). The resin was then treated at 20 °C for 18 h, with 2.5 g of TBAF hydrate in 3 mL of DCM.[72] After washing with DCM and DMF the synthesis was continued using standard Fmoc protocol and workup.

Random Disulfide Bond Formation. Pure, reduced peptides containing pairs of sulfhydryl or selenohydryl groups (1 mg/mL) were oxidized by stirring at rt in 30% DMSO/5% HOAc for 16 h. The solutions were subsequently diluted to a DMSO concentration of <5%, prior to RP-HPLC purification and lyophilization.

Selective Disulfide Bond Formation.[15] Selectively folded peptide isomers of **1** were assembled on Rink (amide) resin. For each of the different isomers one pair of cysteine residues was incorporated into the sequence, using Cys(Trt) protection while the other Cys pair used the orthogonal protection of Cys(Acm). After cleavage and purification of the reduced peptide the first disulfide bond was formed using the standard 30% DMSO/0.1 M NH_4OAc buffer (pH 6) method described above.

The formation of the second disulfide bond was performed by dissolving the purified, singly oxidized di(Acm) peptide at a concentration of 1 mM in 80% acetic acid/water. Iodine (10 equiv) dissolved in a small volume of ethyl acetate was added and the mixture stirred at rt. The progress of the Acm-deprotection and subsequent disulfide bond formation was monitored by direct injection ESMS at regular intervals until completion (∼30−90 min). The reaction was then quenched by addition of ascorbic acid solution (10 mg/mL) resulting in a decolorization of the solution. After dilution with 5 times the volume of water and adjusting to pH 3, the fully oxidized peptide was loaded onto a RP-HPLC column and purified as described below.

HPLC Analysis and Purification. Analytical HPLC runs were performed using a Shimadzu HPLC system LC10A with a dual wavelength UV detector set at 214 and 254 nm. A reversed-phase C-18 column (Zorbax 300-SB C-18; 4.6 mm × 50 mm) with a flow rate of 2 mL/min was used. Gradient elution was performed with the following buffer systems: A, 0.05% TFA in water and B, 0.043% TFA in 90% acetonitrile in water, from 0% B to 80% B in 20 min. The crude peptides were purified by semipreparative HPLC on a Shimadzu HPLC system LC8A associated with a reversed-phase C-18 column (Vydac C-18, 25 cm × 10 mm) running at a flow rate of 5 mL/min with a 1% gradient of 0% B to 40% B. The purity of the final product was evaluated by analytical HPLC (Zorbax 300SB C-18: 4.6 mm × 100 mm) with a flow rate of 1 mL/min and a 1.5% gradient of B (0−45%). The synthesized peptides were all confirmed with >95% purity.

Electrospray Mass Spectrometry (ESMS). Electrospray mass spectra were collected inline during analytical HPLC runs on an Applied Biosystems API-150 spectrometer operating in the positive ion mode with an OR of 20, Rng of 220, and Turbospray of 350 degrees. Masses between 300 and 2200 amu were detected (step 0.2 amu, dwell 0.3 ms).

Plasma Stability Evaluation of Peptides.[18] Stability experiments were performed in triplicate with −80 °C stored Wistar rat plasma. After defrosting at room temperature the plasma was kept on ice. Solids were removed by centrifugation. Peptides were dissolved as a 1 mg/mL solution in sterile PBS buffer (pH 7.4). Of these peptide solutions, an amount of 50 μL was transferred into Eppendorf tubes and 50 μL of the rat plasma supernatant was added. After mixing, the samples were incubated at 37 °C. The initial sample and samples after 1 h, 2 h, 3 h, 4 h, 6 h, and 24 h were quenched with 50 μL of acetonitrile and 400 μL of 2% TFA/water. The quenched samples

DOI: 10.1021/acs.jmedchem.5b00911
J. Med. Chem. 2016, 59, 2381−2395

were vortexed and analyzed by HPLC on a Hypersil Gold analytical column (2.1 mm × 100 mm, 3 nm) using a 5−45% B with a gradient of 2%/min and 0.3 mL flow. Peptide peak areas were integrated and the percent peptide left, compared to the initial, was graphed against the time. Mass spectroscopic evaluation was run in parallel to clearly identify observed fragments.

Peptide Concentration Assessment. Peptide concentration, used in in vitro screening, were calculated based on peak area detected at 214 nm by HPLC. Peak area was calibrated using a peptide standard with known peptide content established by amino acid analysis. Molecular extinction coefficients were calculated for the standard and the peptide of interest applying increments established by Buck et al.[80] By use of the Lambert−Beer law, the peptide concentration is calculated based on absorptions of standard and sample using calculated extinction coefficients.

Cell Culture, Transfection, and Membrane Preparation. CHO-KI cells were cultured in Ham's F12, 10% FBS at 37 °C and 5% CO_2. Transient transfections were performed 24 h after seeding cells at 6 × 10^6 cells in a 150 mm plates using Trans-IT CHO transfection reagent per manufacturer's instructions (Mirus). Briefly, the method involved combining Trans-IT CHO reagent (72 μL) in serum-free Ham's F-12 media incubated for 5 min at room temperature. Following the addition of KOR receptor plasmid (24 μg), this mixture was incubated for 10 min at room temperature. CHO Mojo reagent (16 μL) was added to the mixture and incubated for 15 min at room temperature prior to the addition to the cells.

For KOR membrane preparations the transfected cells were harvested after 24 h by the following method. Confluent 150 mm plates were washed with PBS, harvested by scraping into ice-cold harvest buffer (50 mM Tris-HCl, pH 7.4, 5 mM $MgCl_2$), followed by homogenization with a Polytron homogenizer for 3 min on ice, then centrifugation at 100*g* for 5 min at 4 °C. Supernatants were recovered and centrifuged at 22 000*g* for 1 h at 4 °C. Membrane pellets were resuspended in 0.5 mL of ice-cold harvest buffer containing 10% glycerol and aliquots stored at −80 °C until use. The protein concentration of the membrane preparations was determined by the Bradford method.[81]

Receptor Binding Studies. Receptor binding assays were performed using FlashBlue GPCR scintillation beads using a previously described method.[82] Briefly, FlashBlue GPCR SPA binding assays were performed in 96-well white polystyrene plates with clear flat bottoms (Corning). Radioligands KOR ^{3}H-U69,593 [(5a,7a,8b)-(−)-*N*-methyl-[7-(1-pyrrolidinyl)-1-oxaspiro[4,5]dec-8-yl]benzeneacetamide] (1 nM), DOR ^{3}H-naltrindole (0.4 nM), MOR ^{3}H-diprenorphine (0.2 nM), NOP ^{3}H-nociceptin (0.26 nM)) were added to each membrane preparation, followed by the addition of various concentrations of competing ligands (1 pM to 10 μM) in a total volume of 80 μL containing assay buffer A, B, or C (buffer A, B, 50 mM Tris-HCl, pH 7.4, 5 mM $MgCl_2$, and either 0.1% (A) or 0.5% (B) bovine serum albumin (BSA); or buffer C, 50 mM HEPES, pH 7.4, 1 mM EDTA, 10 mM $MgCl_2$, and 0.5% BSA) (KOR and DOR assays, buffer A; MOR assay, buffer B; NOP assay, buffer C). The final reaction volume per well comprised 20 μL of compound/buffer, 20 μL of FlashBlue GPCR beads (KOR, DOR, and MOR, 100 μg; NOP, 200 μg), 20 μL of membrane (~2 μg), and the assay was initiated by the addition of 20 μL of radioligand. The plate was then sealed with TopSeal-A sealing film and incubated with shaking for 1 h at room temperature. Radioligand binding was then assessed for 30 s/well on a 1450 Microbeta scintillation counter (PerkinElmer). Nonspecific binding was determined in the presence of 10 μM Dynorphin A. Data were analyzed using Prism 6 software (GraphPad Software, San Diego, CA, USA) with curves generated using sigmoidal dose−response analysis.

ERK1/2 Phosphorylation Assay. Alphascreen SureFire phospho-ERK1/2 assay was performed according to the manufacturer's instructions (PerkinElmer). Briefly, cells were harvested 24 h after transfection with 0.05% trypsin−EDTA in phosphate buffered saline (PBS) and transferred to 96-well tissue culture plates at 50 000 cells/well and allowed to settle for 24 h. The following day cells were serum starved in Ham's F-12 media for 12 h at 37 °C and 5% CO_2. Ligands were prepared in serum-free medium and then incubated at room temperature for 10 min with cells. Medium was then removed, and cells were lysed with lysis buffer for 10 min on a shaker. Then 4 μL of lysate was transferred to a white 96-well half area plate (Corning) and incubated in the presence of 7 μL of reaction mix. The plate was sealed with TopSeal-A, transferred to plate shaker for 2 min, then incubated for 2 h at 37 °C. Assay was than measured on an Envision plate reader (PerkinElmer). Data were analyzed using Prism 6 software (GraphPad Software, San Diego, CA, USA) with curves generated using sigmoidal dose−response analysis.

Inhibition of cAMP Production Assay. The inhibition of cAMP production following activation of KOR was measured using the LANCE cAMP assay kit as per manufacturer's instructions (PerkinElmer). Briefly cells were harvested 24 h post-transfection and added to a 96-well white half area plate (Corning) at a final concentration of 3000 cells/well in stimulation buffer (HBSS, 0.1% BSA, 0.5 mM IBMX, 5 mM HEPES, pH 7.4) in a volume of 5 μL. To this 2.5 μL of forskolin (1 μM final concentration) in stimulation buffer was added, followed by 2.5 μL of ligand/stimulation buffer. The plate was then incubated for 30 min at rt. Following incubation, 5 μL of Eu-cAMP tracer solution and 5 μL of anti-cAMP reagent were added and the plate was sealed with TopSeal-A (PerkinElmer) and left to incubate at rt for 1 h. Following incubation, TopSeal-A was removed and plate was read in an Envision plate reader (PerkinElmer). Data were analyzed using Prism 6 software (GraphPad Software, San Diego, CA, USA) with curves generated using sigmoidal dose−response analysis.

Molecular Docking. Docking of the peptide ligand to the orthosteric binding site of KOR was performed with AutoDock. The receptor was checked for parameters like polar hydrogens, assignment of partial atomic Kollman charges, and solvation parameters. Lamarckian genetic algorithm (LGA) implemented in AutoDock tools (ADT) was used for conformational sampling of ligands. In AutoDock, the grid maps were prepared using the AutoGrid utility with 54 × 52 × 48 points, which is sufficiently large to accommodate all active site residues and grid spacing set to 1.0 Å. Docking parameters were kept as per following: number of individuals in the population, 150; maximum number of energy evaluations, 2 500 000; maximum number of generations, 2700; number of GA runs, 20.

Chronic Visceral Hypersensitivity (CVH) Model and Colonic Primary Afferent Recording. Male C57BL/6 mice aged 17 weeks of age and weighing between 28 and 32 g were used for colonic nociceptor studies. Intracolonic trinitrobenzenesulfonic acid (TNBS; 130 μL/mL in 30% ethanol, 0.1 mL bolus) was administered as described previously.[43,83,84] TNBS-treated mice were allowed to recover for 28 days, at which stage inflammation had resolved and chronic colonic afferent mechanical hypersensitivity was evident.[43,85,86] These mice are termed chronic visceral hypersensitivity (CVH) mice.[43,83,84] In vitro single-unit extracellular recordings of action potential discharge were made from splanchnic colonic afferents from C57BL/6 healthy or CVH mice using standard protocols.[43,83,84,87] Baseline mechanosensitivity was determined in response to application of a 2 g Von Frey hair probe to the afferent receptive field for 3 s. This process was repeated 3−4 times, separated each time by 10 s. Mechanosensitivity was then retested after application of KOR agonist, respectively. The KOR agonist was applied to the mucosal surface of the colon for a period of 5 min at each concentration via a small metal ring placed over the receptive field of interest. In some instances data are presented as "change from baseline". This is calculated by determining the change in mechanosensitivity of individual afferents between the normal "baseline" response in healthy or CVH conditions compared to the respective mechanical responses following drug or peptide addition. In the respective study this difference is then averaged across all afferents to obtain a final mean ± SEM of "change in response from baseline". Data are presented as spikes/s and are expressed as mean ± SEM. Data were analyzed using Prism 6 software (GraphPad Software, San Diego, CA, USA), and statistical analysis resulting in data output in Figure 7A,B,D was performed using one-way ANOVA followed by Bonferroni's post hoc test. Data outputs shown in Figure 7C were statistically analyzed using two-way ANOVA

DOI: 10.1021/acs.jmedchem.5b00911
J. Med. Chem. 2016, 59, 2381−2395

followed by Holm−Sidak's post hoc test. Data outputs shown in Figure 7E (CVH baseline Vs KOR agonist **39** and also CVH baseline Vs NorBNI + KOR agonist **39**) were analyzed using a paired *t* test. Differences between specific drug concentrations and baseline responses were considered significant at (*) $P < 0.05$, (**) $P < 0.01$, (***) $P < 0.001$, or (****) $P < 0.0001$. *n* indicates the number of individual nociceptors. Experiments involving animals were approved by the Animal Ethics Committees of The University of Adelaide and the South Australian Health and Medical Research Institute (SAHMRI).

■ ASSOCIATED CONTENT

Supporting Information

The Supporting Information is available free of charge on the ACS Publications website at DOI: 10.1021/acs.jmedchem.5b00911.

Additional information on product purity, product masses, and k' values, exemplary dose−response curve showing full agonist behavior of initial lead peptide **1** and advanced analogue **39** compared to dynA (1−17) (PDF)

■ AUTHOR INFORMATION

Corresponding Authors

*A.B.: phone, 61 7 3346 2985; e-mail, a.brust@imb.uq.edu.au.
*R.J.L.: phone, 61 7 3346 2984; e-mail, r.lewis@imb.uq.edu.au.

Notes

The authors declare no competing financial interest.

■ ACKNOWLEDGMENTS

S.M.B is an NHMRC R. D. Wright Biomedical Research Fellow, and R.J.L. and P.F.A. are NHMRC Principal Research Fellows. This work was supported by NHMRC Program Grant 569927.

■ ABBREVIATIONS USED

KOR, κ opioid receptor; MOR, μ opioid receptor; DOR, δ opioid receptor; NOP, nociceptin/orphanin FQ receptor; U, L-pyroglutamic acid; [ACC], (3*S*)-3-amino-1-carboxymethyl-caprolactam; [NAL], L-1-naphthylalanine; [CHA], L-cyclohexylalanine; [CHG], L-cyclohexylglycine; [DAP], L-β-aminoalanine; [CIT], L-citrulline; [NMC], *N*-methyl-L-cysteine; [TIC], 1,2,3,4-L-tetrahydroisoquinoline-3-carboxylic acid; [HCY], L-homocysteine; [PEN], L-penicillamine; [ANC], 3-aminonaphthalene-2-carboxylic acid; [QIN], 3-quinolinecarboxylic acid; [TIQ], L-tetrahydroisoquinoline-1-carboxylic acid; [SEC], L-selenocysteine; [MEG], *N*-mercaptoethylglycine; [MPC], (2*S*,4*S*)-4-mercaptoproline; 4-Cl-Bz, 4-chlorobenzyl; -CH_2-NH, reduced amide bond; HBTU, *N*,*N*,*N*′,*N*′-tetramethyl-*O*-(1*H*-benzotriazol-1-yl)uranium hexafluorophosphate); MSNT, 1-(2-mesitylensulfonyl)-3-nitro-1*H*-1,2,4-triazole; EDT, ethanedithiol; TIPS, triisopropylsilane; TFA, trifluoroacetic acid; DCC, *N*,*N*′-dicyclohexylcarbodiimide; NEM, *N*-ethylmorpholine; DMAP, 4-dimethylaminopyridine; DMSO, dimethylsulfoxide; Acm, acetamidomethyl; RP-HPLC, reversed-phase high-performance liquid chromatography; LC−MS, liquid chromatography coupled mass spectrometry; NMR, nuclear magnetic resonance; NOESY, nuclear Overhauser enhancement spectroscopy; GPCR, G-protein-coupled receptor; CHO, Chinese hamster ovary; TNBS, trinitrobenzenesulfonic acid; ERK, extracellular signal-regulated kinase

Carboxylic Acid Capping Groups

Bz, benzyl; Nz, naphthyl-2-carboxyl; Bnz, benzoyl

■ ADDITIONAL NOTE

Natural occurring amino acids are abbreviated to standard single or three letter codes: capital letters represent L-amino acids, and lower case letters represent D-amino acids. Unnatural amino acids are indicated using a three letter code in square brackets. Aromatic substitution is indicated by ring position number and nature of substituent.

■ REFERENCES

(1) Lazcano-Perez, F.; Roman-Gonzalez, S. A.; Sanchez-Puig, N.; Arreguin-Espinosa, R. Bioactive peptides from marine organisms: a short overview. *Protein Pept. Lett.* **2012**, *19*, 700−707.
(2) Haefner, B. Drugs from the deep: marine natural products as drug candidates. *Drug Discovery Today* **2003**, *8*, 536−544.
(3) Lewis, R. J.; Dutertre, S.; Vetter, I.; Christie, M. J. Conus venom peptide pharmacology. *Pharmacol. Rev.* **2012**, *64*, 259−298.
(4) Jin, A.-H.; Dutertre, S.; Kaas, Q.; Lavergne, V.; Kubala, P.; Lewis, R. J.; Alewood, P. F. Transcriptomic messiness in the venom duct of Conus miles contributes to conotoxin diversity. *Mol. Cell. Proteomics* **2013**, *12*, 3824−3833.
(5) Davis, J.; Jones, A.; Lewis, R. J. Remarkable inter- and intra-species complexity of conotoxins revealed by LC/MS. *Peptides* **2009**, *30*, 1222−1227.
(6) Vetter, I.; Lewis, R. J. Therapeutic potential of cone snail venom peptides (conopeptides). *Curr. Top. Med. Chem.* **2012**, *12*, 1546−1552.
(7) Lewis, R. J. Conotoxins: molecular and therapeutic targets. *Prog. Mol. Subcell. Biol.* **2009**, *46*, 45−65.
(8) Lewis, R. J. Conotoxin venom peptide therapeutics. *Adv. Exp. Med. Biol.* **2009**, *655*, 44−48.
(9) King, G. F. Venoms as a platform for human drugs: translating toxins into therapeutics. *Expert Opin. Biol. Ther.* **2011**, *11*, 1469−1484.
(10) Lewis, R. J.; Garcia, M. L. Therapeutic potential of venom peptides. *Nat. Rev. Drug Discovery* **2003**, *2*, 790−802.
(11) Prashanth, J. R.; Brust, A.; Jin, A.-H.; Alewood, P. F.; Dutertre, S.; Lewis, R. J. Cone snail venomics: from novel biology to novel therapeutics. *Future Med. Chem.* **2014**, *6*, 1659−1675.
(12) McGivern, J. G. Ziconotide: a review of its pharmacology and use in the treatment of pain. *Neuropsychiatr. Dis. Treat.* **2007**, *3*, 69−85.
(13) Schmidtko, A.; Loetsch, J.; Freynhagen, R.; Geisslinger, G. Ziconotide for treatment of severe chronic pain. *Lancet* **2010**, *375*, 1569−1577.
(14) Ragnarsson, L.; Wang, C.-I.A.; Andersson, Å.; Fajarningsih, D.; Monks, T.; Brust, A.; Rosengren, K. J.; Lewis, R. J. Conopeptide ρ-TIA defines a new allosteric site on the extracellular surface of the α1B-adrenoceptor. *J. Biol. Chem.* **2013**, *288*, 1814−1827.
(15) Drew, L. J.; Rugiero, F.; Cesare, P.; Gale, J. E.; Abrahamsen, B.; Bowden, S.; Heinzmann, S.; Robinson, M.; Brust, A.; Colless, B.; Lewis, R. J.; Wood, J. N. High-threshold mechanosensitive ion channels blocked by a novel conopeptide mediate pressure-evoked pain. *PLoS One* **2007**, *2*, e515.
(16) Sharpe, I. A.; Thomas, L.; Loughnan, M.; Motin, L.; Palant, E.; Croker, D. E.; Alewood, D.; Chen, S.; Graham, R. M.; Alewood, P. F.; Adams, D. J.; Lewis, R. J. Allosteric α1-adrenoreceptor antagonism by conopeptide ρ-TIA. *J. Biol. Chem.* **2003**, *278*, 34451−34457.
(17) Brust, A.; Palant, E.; Croker, D. E.; Colless, R.; Drinkwater, R.; Patterson, B.; Schroeder, C. I.; Wilson, D.; Nielsen, C. K.; Smith, M. T.; Alewood, D.; Alewood, P. F.; Lewis, R. J. chi-Conopeptide Pharmacophore Development: Toward a novel class of norepinephrine transporter inhibitor (Xen2174) for pain. *J. Med. Chem.* **2009**, *52*, 6991−7002.
(18) Brust, A.; Wang, C.-I. A.; Daly, N. L.; Kennerly, J.; Sadeghi, M.; Christie, M. J.; Lewis, R. J.; Mobli, M.; Alewood, P. F. Vicinal disulfide constrained cyclic peptidomimetics: a turn mimetic scaffold targeting the norepinephrine transporter. *Angew. Chem., Int. Ed.* **2013**, *52*, 12020−12023.

DOI: 10.1021/acs.jmedchem.5b00911
J. Med. Chem. 2016, 59, 2381−2395

(19) Brust, A.; Tickle, A. E. High-throughput synthesis of conopeptides: a safety-catch linker approach enabling disulfide formation in 96-well format. *J. Pept. Sci.* **2007**, *13*, 133−141.
(20) Arner, S. Opioids and long-lasting pain conditions: 25-year perspective on mechanism-based treatment strategies. *Pain Rev.* **2000**, *7*, 81−96.
(21) Sadhasivam, S.; Chidambaran, V. Pharmacogenomics of opioids and perioperative pain management. *Pharmacogenomics* **2012**, *13*, 1719−1740.
(22) Kalso, E.; Edwards, J. E.; Moore, R. A.; McQuay, H. J. Opioids in chronic non-cancer pain: systematic review of efficacy and safety. *Pain* **2004**, *112*, 372−380.
(23) Ballantyne, J. C.; Shin, N. S. Efficacy of opioids for chronic pain: a review of the evidence. *Clin. J. Pain* **2008**, *24*, 469−478.
(24) McDonald, J.; Lambert, D. G. Opioid mechanisms and opioid drugs. *Anaesth. Intensive Care* **2013**, *14*, 505−509.
(25) Feng, Y.; He, X.; Yang, Y.; Chao, D.; Lazarus, L. H.; Xia, Y. Current research on opioid receptor function. *Curr. Drug Targets* **2012**, *13*, 230−246.
(26) Dietis, N.; Rowbotham, D. J.; Lambert, D. G. Opioid receptor subtypes: fact or artifact? *Br. J. Anaesth.* **2011**, *107*, 8−18.
(27) Zaveri, N. T. The nociceptin/orphanin FQ receptor (NOP) as a target for drug abuse medications. *Curr. Top. Med. Chem.* **2011**, *11*, 1151−1156.
(28) Chiou, L. C.; Liao, Y. Y.; Fan, P. C.; Kuo, P. H.; Wang, C. H.; Riemer, C.; Prinssen, E. P. Nociceptin/orphanin FQ peptide receptors: pharmacology and clinical implications. *Curr. Drug Targets* **2007**, *8*, 117−135.
(29) Aldrich, J. V.; McLaughlin, J. P. Peptide kappa opioid receptor ligands: potential for drug development. *AAPS J.* **2009**, *11*, 312−322.
(30) Christo, P. J. Opioid effectiveness and side effects in chronic pain. *Anesthesiol. Clin. North Am.* **2003**, *21*, 699−713.
(31) Bates, J. J.; Foss, J. F.; Murphy, D. B. Are peripheral opioid antagonists the solution to opioid side effects? *Anesth. Analg.* **2004**, *98*, 116−122.
(32) Kivell, B.; Prisinzano, T. E. Kappa opioids and the modulation of pain. *Psychopharmacology* **2010**, *210*, 109−119.
(33) Deuis, J. R.; Whately, E.; Brust, A.; Inserra, M. C.; Asvadi, N. H.; Lewis, R. J.; Alewood, P. F.; Cabot, R. J.; Vetter, I. Activation of κ opioid receptors in cutaneous nerve endings by Conorphin-1, a novel subtype-selective conopeptide, does not mediate peripheral analgesia. *ACS Chem. Neurosci.* **2015**, *6*, 1751.
(34) Auh, Q. S.; Ro, J. Y. Effects of peripheral κ opioid receptor activation on inflammatory mechanical hyperalgesia in male and female rats. *Neurosci. Lett.* **2012**, *524*, 111−115.
(35) Butelman, E. R.; Yuferov, V.; Kreek, M. J. κ-opioid receptor/dynorphin system: genetic and pharmacotherapeutic implications for addiction. *Trends Neurosci.* **2012**, *35*, 587−596.
(36) Wee, S.; Koob, G. F. The role of the dynorphin-κ opioid system in the reinforcing effects of drugs of abuse. *Psychopharmacology* **2010**, *210*, 121−135.
(37) Metz, M.; Staender, S. Chronic pruritus - pathogenesis, clinical aspects and treatment. *J. Eur. Acad. Dermatol. Venereol.* **2010**, *24*, 1249−1260.
(38) Knoll, A. T.; Carlezon, W. A. Dynorphin, stress, and depression. *Brain Res.* **2010**, *1314*, 56−73.
(39) Tejeda, H. A.; Shippenberg, T. S.; Henriksson, R. The dynorphin/κ-opioid receptor system and its role in psychiatric disorders. *Cell. Mol. Life Sci.* **2012**, *69*, 857−896.
(40) Wang, Y.-H.; Sun, J.-F.; Tao, Y.-M.; Chi, Z.-Q.; Liu, J.-G. The role of κ-opioid receptor activation in mediating antinociception and addiction. *Acta Pharmacol. Sin.* **2010**, *31*, 1065−1070.
(41) Fichna, J.; Schicho, R.; Janecka, A.; Zjawiony, J. K.; Storr, M. Selective natural κ opioid and cannabinoid receptor agonists with a potential role in the treatment of gastrointestinal dysfunction. *Drug News Perspect.* **2009**, *22*, 383−392.
(42) Mangel, A. W.; Williams, V. S. Asimadoline in the treatment of irritable bowel syndrome. *Expert Opin. Invest. Drugs* **2010**, *19*, 1257−1264.
(43) Hughes, P. A.; Castro, K. J.; Harrington, A.; Isaacs, N.; Moretta, M.; Hicks, G.; Urso, D.; Brierley, S. Increased kappa-opioid receptor expression and function during chronic visceral hypersensitivity. *Gut* **2014**, *63*, 1199−1200.
(44) Naqvi, T.; Haq, W.; Mathur, K. B. Structure-activity relationship studies of dynorphin A and related peptides. *Peptides* **1998**, *19*, 1277−1292.
(45) Meng, F.; Hoversten, M. T.; Thompson, R. C.; Taylor, L.; Watson, S. J.; Akil, H. A chimeric study of the molecular basis of affinity and selectivity of the κ and the δ opioid receptors: Potential role of extracellular domains. *J. Biol. Chem.* **1995**, *270*, 12730−12736.
(46) Lapalu, S.; Moisand, C.; Mazarguil, H.; Cambois, G.; Mollereau, C.; Meunier, J.-C. Comparison of the structure-activity relationships of nociceptin and dynorphin A using chimeric peptides. *FEBS Lett.* **1997**, *417*, 333−336.
(47) Schlechtingen, G.; DeHaven, R. N.; Daubert, J. D.; Cassel, J. A.; Chung, N. N.; Schiller, P. W.; Taulane, J. P.; Goodman, M. Structure-activity relationships of dynorphin A analogues modified in the address sequence. *J. Med. Chem.* **2003**, *46*, 2104−2109.
(48) Wan, X.-H.; Huang, X. Q.; Zhou, D. H.; Jiang, H. L.; Chen, K. X.; Chi, Z. Q. Building 3D-structural model of kappa opioid receptor and studying its interaction mechanism with dynorphin A(1-8). *Acta Pharmacol. Sin.* **2000**, *21*, 701−708.
(49) Wu, H.; Wacker, D.; Mileni, M.; Katritch, V.; Han, G. W.; Vardy, E.; Liu, W.; Thompson, A. A.; Huang, X.-P.; Carroll, F. I.; Mascarella, S. W.; Westkaemper, R. B.; Mosier, P. D.; Roth, B. L.; Cherezov, V.; Stevens, R. C. Structure of the human χ-opioid receptor in complex with JDTic. *Nature* **2012**, *485*, 327−332.
(50) Vardy, E.; Mosier, P. D.; Frankowski, K. J.; Wu, H.; Katritch, V.; Westkaemper, R. B.; Aube, J.; Stevens, R. C.; Roth, B. L. Chemotype-selective modes of action of kappa-opioid receptor agonists. *J. Biol. Chem.* **2013**, *288*, 34470−34483.
(51) Riviere, P. J. M. Peripheral kappa-opioid agonists for visceral pain. *Br. J. Pharmacol.* **2004**, *141*, 1331−1334.
(52) Camilleri, M. Novel pharmacology: asimadoline, a kappa-opioid agonist, and visceral sensation. *Neurogastroenterol. Motil.* **2008**, *20*, 971−979.
(53) Vanderah, T. W.; Schteingart, C. D.; Trojnar, J.; Junien, J.-L.; Lai, J.; Rivier, P. J.-M. Fe200041 (D-Phe-D-Phe-D-Nle-D-Arg-NH2): A peripheral efficacious κ opioid agonist with unprecedented selectivity. *J. Pharmacol. Exp. Ther.* **2004**, *310*, 326−333.
(54) Dooley, C. T.; Ny, P.; Bidlack, J. M.; Houghten, R. A. Selective ligands for the mu, delta, and kappa opioid receptors identified from a single mixture based tetrapeptide positional scanning combinatorial library. *J. Biol. Chem.* **1998**, *273*, 18848−18856.
(55) Luo, S.; Zhangsun, D.; Zhang, B.; Chen, X.; Feng, J. Direct cDNA cloning of novel conotoxins of the T-superfamily from Conus textile. *Peptides* **2006**, *27*, 2640−2646.
(56) Venkatakrishnan, A. J.; Deupi, X.; Lebon, G.; Tate, C. G.; Schertler, G. F.; Babu, M. M. Molecular signatures of G-protein-coupled receptors. *Nature* **2013**, *494*, 185−194.
(57) Thomsen, W.; Frazer, J.; Unett, D. Functional assays for screening GPCR targets. *Curr. Opin. Biotechnol.* **2005**, *16*, 655−665.
(58) Siehler, S. Cell-based assays in GPCR drug discovery. *Biotechnol. J.* **2008**, *3*, 471−483.
(59) Osmond, R. I.; Sheehan, A.; Borowicz, R.; Barnett, E.; Harvey, G.; Turner, C.; Brown, A.; Crouch, M. F.; Dyer, A. R. GPCR screening via ERK 1/2: a novel platform for screening G protein-coupled receptors. *J. Biomol. Screening* **2005**, *10*, 730−737.
(60) Al-Hasani, R.; Bruchas, M. R. Molecular mechanisms of opioid receptor-dependent signaling and behavior. *Anesthesiology* **2011**, *115*, 1363−1381.
(61) Carugo, O.; Čemažar, M.; Zahariev, S.; Hudáky, I.; Gáspári, Z.; Perczel, A.; Pongor, S. Vicinal disulfide turns. *Protein Eng., Des. Sel.* **2003**, *16*, 637−639.
(62) Hudaky, I.; Gáspári, Z.; Carugo, O.; Čemažar, M.; Pongor, S.; Perczel, A. Vicinal disulfide bridge conformers by experimental methods and by ab initio and DFT molecular computations. *Proteins: Struct., Funct., Genet.* **2004**, *55*, 152−168.

DOI: 10.1021/acs.jmedchem.5b00911
J. Med. Chem. 2016, 59, 2381−2395

(63) Blum, A. P.; Gleitsman, K. R.; Lester, H. A.; Dougherty, D. A. Evidence for an extended hydrogen bond network in the binding site of the nicotinic receptor: role of the vicinal disulfide of the α1 subunit. *J. Biol. Chem.* **2011**, *286*, 32251−32258.
(64) Gunning, S. J.; Maggio, F.; Windley, M. J.; Valenzuela, S. M.; King, G. F.; Nicholson, G. M. The Janus-faced atracotoxins are specific blockers of invertebrate KCa channels. *FEBS J.* **2008**, *275*, 4045−4059.
(65) Mobli, M.; de Araújo, A. D.; Lambert, L. K.; Pierens, G. K.; Windley, M. J.; Nicholson, G. M.; Alewood, P. F.; King, G. F. Direct visualization of disulfide bonds through Diselenide proxies using 77Se NMR spectroscopy. *Angew. Chem., Int. Ed.* **2009**, *48*, 9312−9314.
(66) Gehrmann, J.; Alewood, P. F.; Craik, D. J. Structure determination of the three disulfide bond isomers of alpha-conotoxin GI: a model for the role of disulfide bonds in structural stability. *J. Mol. Biol.* **1998**, *278*, 401−415.
(67) Wang, X.-h.; Connor, M.; Smith, R.; Maciejewski, M. W.; Howden, M. E. H.; Nicholson, G. M.; Christie, M. J.; King, G. F. Discovery and characterization of a family of insecticidal neurotoxins with a rare vicinal disulfide bridge. *Nat. Struct. Biol.* **2000**, *7*, 505−513.
(68) Ruggles, E. L.; Deker, P. B.; Hondal, R. J. Synthesis, redox properties, and conformational analysis of vicinal disulfide ring mimics. *Tetrahedron* **2009**, *65*, 1257−1267.
(69) Zimmermann, J.; Kuehne, R.; Sylvester, M.; Freund, C. Redox-regulated conformational changes in an SH3 domain. *Biochemistry* **2007**, *46*, 6971−6977.
(70) Biron, E.; Chatterjee, J.; Kessler, H. Optimized selective N-methylation of peptides on solid support. *J. Pept. Sci.* **2006**, *12*, 213−219.
(71) Guichard, G.; Briand, J. P.; Friede, M. Synthesis of arginine aldehydes for the preparation of pseudopeptides. *Pept. Res.* **1993**, *6*, 121−124.
(72) Ueki, M.; Ikeo, T.; Slaninova, J.; Iwadate, M.; Asakura, T.; Williamson, M. P. Solid phase synthesis and biological activities of [Arg8]-vasopressin methylenedithioether. *Bioorg. Med. Chem. Lett.* **1999**, *9*, 1767−1772.
(73) Muttenthaler, M.; Alewood, P. F. Selenopeptide chemistry. *J. Pept. Sci.* **2008**, *14*, 1223−1239.
(74) Muttenthaler, M.; Alewood, P. F. Directed folding of alpha-conotoxins using selenocysteine. *J. Pept. Sci.* **2006**, *12*, 83−83.
(75) Kenakin, T. New concepts in pharmacological efficacy at 7TM receptors: IUPHAR review 2. *Br. J. Pharmacol.* **2013**, *168*, 554−575.
(76) Pradhan, A. A.; Smith, M. L.; Kieffer, B. L.; Evans, C. J. Ligand-directed signaling within the opioid receptor family. *Br. J. Pharmacol.* **2012**, *167*, 960−969.
(77) Delvaux, M.; Beck, A.; Jacob, J.; Bouzamondo, H.; Weber, F. T.; Frexinos, J. Effect of asimadoline, a kappa opioid agonist, on pain induced by colonic distension in patients with irritable bowel syndrome. *Aliment. Pharmacol. Ther.* **2004**, *20*, 237−246.
(78) Mangel, A. W.; Hicks, G. A. Asimadoline and its potential for the treatment of diarrhea-predominant irritable bowel syndrome: a review. *Clin. Exp. Gastroenterol.* **2012**, *5*, 1−10.
(79) Alewood, P. F.; Alewood, D.; Miranda, L.; Love, S.; Meutermans, W.; Wilson, D. Rapid in situ neutralization protocols for Boc and Fmoc solid-phase chemistries. *Methods Enzymol.* **1997**, *289*, 14−29.
(80) Buck, M. A.; Olah, T. A.; Weitzmann, C. J.; Cooperman, B. S. Protein estimation by the product of integrated peak area and flow rate. *Anal. Biochem.* **1989**, *182*, 295−299.
(81) Bradford, M. M. A rapid and sensitive method for the quantitation of microgram quantities of protein utilizing the principle of protein-dye binding. *Anal. Biochem.* **1976**, *72*, 248−254.
(82) Dutertre, S.; Croker, D.; Daly, N. L.; Andersson, Å.; Muttenthaler, M.; Lumsden, N. G.; Craik, D. J.; Alewood, P. F.; Guillon, G.; Lewis, R. J. Conopressin-T from Conus tulipa reveals an antagonist switch in vasopressin-like peptides. *J. Biol. Chem.* **2008**, *283*, 7100−7108.
(83) Castro, J.; Jin, H.; Jacobson, S.; Hannig, G.; Mann, E.; Cohen, M. B.; MacDougall, J. E.; Lavins, B. J.; Kurtz, C. B.; Silos-Santiago, I.; Johnston, J. M.; Currie, M. G.; Blackshaw, L. A.; Brierley, S. M. Linaclotide inhibits colonic nociceptors and relieves abdominal pain via guanylate cyclase-C and extracellular cyclic guanosine 3′,5′-monophosphate. *Gastroenterology* **2013**, *145*, 1334−1346.
(84) de Araujo, A. D.; Mobli, M.; Castro, J.; Harrington, A. M.; Vetter, I.; Dekan, Z.; Muttenthaler, M.; Wan, J.; Lewis, R. J.; King, G. F.; Brierley, S. M.; Alewood, P. F. Selenoether oxytocin analogues have analgesic properties in a mouse model of chronic abdominal pain. *Nat. Commun.* **2014**, *5*, 3165−3176.
(85) Brierley, S. M.; Linden, D. R. Neuroplasticity and dysfunction after gastrointestinal inflammation. *Nat. Rev. Gastroenterol. Hepatol.* **2014**, *11*, 611−627.
(86) Brierley, S. M.; Hughes, P. A.; Page, A. J.; Kwan, K. Y.; Martin, C. M.; O'Donnell, T. A.; Cooper, N. J.; Harrington, A. M.; Adam, B.; Liebregts, T.; Holtmann, G.; Corey, D. P.; Rychkov, G. Y.; Blackshaw, L. A. The ion channel TRPA1 is required for normal mechanosensation and is modulated by algesic stimuli. *Gastroenterology* **2009**, *137*, 2084−2095.
(87) Brierley, S. M.; Jones, R. C., III; Gebhart, G. F.; Blackshaw, L. A. Splanchnic and pelvic mechanosensory afferents signal different qualities of colonic stimuli in mice. *Gastroenterology* **2004**, *127*, 166−178.

DOI: 10.1021/acs.jmedchem.5b00911
J. Med. Chem. 2016, 59, 2381−2395